Received: 23 November 2023 | Revised: 21 February 2024 | Accepted: 23 February 2024

DOI: 10.1111/bph.16366

RESEARCH ARTICLE

Signalling switches maintain intercellular communication in the vascular endothelium

Charlotte Buckley | Matthew D. Lee | Xun Zhang | Calum Wilson | John G. McCarron

Strathclyde Institute of Pharmacy and Biomedical Sciences, University of Strathclyde, Glasgow, UK

Correspondence
John G. McCarron, Strathclyde Institute of Pharmacy and Biomedical Science, 161 Cathedral Street, Glasgow G4 0RE, UK.
Email: john.mccarron@strath.ac.uk

Funding information
British Heart Foundation, Grant/Award Numbers: RG/F/20/110007, PG/20/9/34859

Abstract

Background and Purpose: The single layer of cells lining all blood vessels, the endothelium, is a sophisticated signal co-ordination centre that controls a wide range of vascular functions including the regulation of blood pressure and blood flow. To co-ordinate activities, communication among cells is required for tissue level responses to emerge. While a significant form of communication occurs by the propagation of signals between cells, the mechanism of propagation in the intact endothelium is unresolved.

Experimental Approach: Precision signal generation and targeted cellular manipulation was used in conjunction with high spatiotemporal mesoscale Ca^{2+} imaging in the endothelium of intact blood vessels.

Key Results: Multiple mechanisms maintain communication so that Ca^{2+} wave propagation occurs irrespective of the status of connectivity among cells. Between adjoining cells, regenerative IP_3-induced IP_3 production transmits Ca^{2+} signals and explains the propagated vasodilation that underlies the increased blood flow accompanying tissue activity. The inositide is itself sufficient to evoke regenerative phospholipase C-dependent Ca^{2+} waves across coupled cells. None of gap junctions, Ca^{2+} diffusion or the release of extracellular messengers is required to support this type of intercellular Ca^{2+} signalling. In contrast, when discontinuities exist between cells, ATP released as a diffusible extracellular messenger transmits Ca^{2+} signals across the discontinuity and drives propagated vasodilation.

Conclusion and Implications: These results show that signalling switches underlie endothelial cell-to-cell signal transmission and reveal how communication is maintained in the face of endothelial damage. The findings provide a new framework for understanding wave propagation and cell signalling in the endothelium.

KEYWORDS
blood vessels, calcium signalling, calcium waves, cell communication, endothelium, vascular tone

Abbreviations: AM, acetoxymethyl ester; EGTA, ethylene glycol tetra-acetic acid; FRAP, Fluorescent recovery after photobleaching; NP, nitrophenyl; PPs, physiological saline solution.

1 | INTRODUCTION

Communication between cells in the endothelium is critical in the control of numerous cardiovascular functions that include the regulation of blood pressure and flow, blood fluidity changes, angiogenesis, alteration of vascular permeability, mediating immune and inflammatory responses. For example, the endothelium regulates local blood flow in the process referred to as 'functional hyperaemia'. The co-ordinated processes in functional hyperaemia lead to dynamic regulation of local blood flow that accommodates the ever-changing metabolic requirements of tissues (Domeier & Segal, 2007; Longden et al., 2017, 2021; Tallini et al., 2007; Uhrenholt et al., 2007). The endothelium controls functional hyperaemia by generating the signals that trigger dilation of small arteries in tissues and by conducting dilatory signals to larger arteries, against the direction of blood flow, in the process referred to as ascending vasodilation. To control this process, endothelial cells communicate over distance, but the mechanisms of signal transmission are unresolved.

Important molecular components for signal transmission and transduction are the **phospholipase C**, **IP_3 receptor (IP_3R)** signalling cascade. The IP_3R transduction cascade underlies numerous endothelial intracellular processes that include control of gene expression, exocytosis and metabolism. This signalling pathway also contributes a significant form of intercellular communication by generating travelling spatial gradients of Ca^{2+} ('Ca^{2+} waves') that move from activated cells across long distances to coordinate endothelial function (Boitano et al., 1992; Isakson et al., 2007). Currently, there are two major competing hypotheses to explain transmission of Ca^{2+} waves across cells. The first requires structural proximity of cells and diffusion of intracellular messengers between them, via specialized endothelial cell couplings referred to as 'gap junctions'. The second hypothesis proposes that Ca^{2+} waves may occur by the regenerative release of extracellular messengers from activated cells. In this case, communication may occur over relatively long distances and structural proximity of cells is not required.

There have been several reports of the transmission of Ca^{2+} waves via gap junction coupling. Gap junctions are formed by the assembly of **connexin** multimer units across adjacent cell membranes (Bennett et al., 1991). The pore formed in a gap junction is large enough to permit the transfer of signalling molecules (Figueroa et al., 2004; Saez et al., 2003), such as **IP_3** (Leybaert et al., 1998; Sanderson, 1995) and Ca^{2+} (Robb-Gaspers & Thomas, 1995; Zimmermann & Walz, 1999). To generate intercellular Ca^{2+} waves, gap junctions are proposed to permit diffusion of IP_3 between cells, which evokes Ca^{2+} release from the endoplasmic reticulum and, as a result, Ca^{2+}-induced IP_3 production (Thomas et al., 1996). The generated IP_3 diffuses into the next cell, also via gap junctions, to repeat the process. The presence of connexins in the endothelium is firmly established (Pohl, 2020) and a role for gap junctions in cell communication is clear in several settings (Charles et al., 1992; de Wit et al., 2000; Figueroa & Duling, 2008; Krüger et al., 2002; Pohl, 2020; Simon & McWhorter, 2003; Wölfle et al., 2007; Zhu et al., 1991). However, the functional role of connexins is often investigated using pharmacological agents or protein knockouts that may inhibit Ca^{2+} waves independently of connexin and gap junction function (Buckley et al., 2021; Chepkova et al., 2008; Suadicani et al., 2006). The widely used gap junction blockers **carbenoxolone** and **18β-glycyrrhetinic acid**, for example, also block IP_3R and depolarize mitochondria at the concentrations used to block connexin function (Buckley et al., 2021; Salvi et al., 2005; Wang et al., 2014). These additional actions of the inhibitors result in widespread effects on cell signalling beyond the role of gap junctions (Buckley et al., 2021).

The involvement of a diffusible messenger, such as **ATP**, has been shown to drive Ca^{2+} wave propagation in some cell types and certain vascular beds (Cotrina et al., 1998; Guthrie et al., 1999; Hassinger et al., 1996; Osipchuk & Cahalan, 1992; Toma et al., 2008). In these settings, ATP is released from cells via connexin pores or **pannexin channels** (Bao et al., 2004), binding to **P2Y receptors** on neighbouring cells leading to Ca^{2+} release from the internal store. The diffusion and regenerative release of ATP extracellularly leads to sequential changes in intracellular Ca^{2+} in nearby cells. These types of Ca^{2+} waves are able to cross distances in which there are no direct connections between cells (Cotrina et al., 1998; Gomes, Srinivas, Vereecke, & Himpens, 2005; Guthrie et al., 1999; Hassinger et al., 1996).

An understanding of Ca^{2+} wave propagation is critical to an appreciation of the communication necessary to control cardiovascular function, particularly because cell communication in the endothelium is altered in vascular disease conditions such as hypertension (de Wit et al., 2003; Kurjiaka, 2004). While much has been achieved, the difficulties in experimentally addressing cell–cell communication and Ca^{2+} wave propagation in native tissue has limited understanding and the precise mechanisms are still unresolved. In the present study, we report that two mechanisms are able to contribute to Ca^{2+} wave propagation in the endothelium in intact arteries. Where there is adjacent structural proximity of cells, a

What is already known

- Endothelial cells are specialized to detect specific stimuli and control virtually all cardiovascular activities.
- Communication across endothelial cells shares information so that a coordinated cardiovascular response occurs.

What does this study add

- We demonstrate that failsafe communication is maintained by two independent mechanisms.
- Intact endothelium, self-renewing IP_3-induced IP_3 production maintains cell-to-cell communication, while diffusible messengers bridge cell discontinuities.

What is the clinical significance

- In endothelium, intercellular signalling switches maintain the robust and sensitive communication necessary for cardiovascular function.

novel regenerative IP_3-induced IP_3 production is critical in the propagation of Ca^{2+} waves. However, gap junctions, Ca^{2+} diffusion or release of extracellular messengers do not contribute to this type of communication. When adjacent structural proximity of cells is disrupted and there are discontinuities between cells, release of extracellular messengers transmits intercellular Ca^{2+} signals across these discontinuities. These findings reveal that intercellular signalling in the endothelium may switch between multiple pathways to maintain the communication among cells that is required to control cardiovascular function.

2 | METHODS

2.1 | Animals

All animal husbandry and causing death were carried out in accordance with the prior approval of the University of Strathclyde Animal Welfare and Ethical Review Body and under relevant UK Home Office Regulations (Schedule 1 of the Animals [Scientific Procedures] Act 1986, UK). Strathclyde biological procedures unit is a conventional facility that undertakes FELASA quarterly health monitoring. Animal studies are reported in compliance with the ARRIVE guidelines (Percie Du Sert et al., 2020) and with the recommendations made by the *British Journal of Pharmacology* (Lilley et al., 2020).

Male (unless otherwise stated) Sprague–Dawley rats (10–12 weeks old; 250–300 g), from an in-house colony, were used for the study. The animals were housed three per cage and the cage type was North Kent Plastic model RC2F with nesting material 'Sizzle Nest'. A 12:12 light dark cycle was used with a temperature range of 19–23°C (set point 21°C) and humidity levels between 45% and 65%. Animals had free access to fresh water and SDS diet RM1 (rodent maintenance). The enrichment in the cages was aspen wood chew sticks and hanging huts. Animals were killed by cervical dislocation and death was confirmed by exsanguination. The mesenteric bed was removed. All experiments were performed using first- or second-order mesenteric arteries unless otherwise indicated. Controls and experimental treatments were carried out in the same tissue, so blinding and randomization were not used. Group sizes were designed to be equal.

2.2 | Mesenteric artery preparation and mounting

Dissected arteries were opened longitudinally and pinned out to expose the endothelial layer, either on Sylgard blocks (for use on inverted microscopes) or in custom-designed baths with Sylgard lining the base (for upright microscopes) using 50-μm diameter pins (Lee et al., 2018; Wilson, Lee, & McCarron, 2016; Wilson, Saunter, et al., 2016a, 2016b). Dissection and experiments were carried out in a physiological saline solution (PS1S: 145-mM NaCl, 2-mM MOPS (3-(*N*-morpholino)propanesulfonic acid), 4.7-mM KCl, 1.2-mM NaH_2PO4, 5-mM Glucose, 0.02-mM EDTA, 1.17-mM MgCl, 2-mM CaCl, pH 7.4). Physiological saline solution (PSS) or a Ca^{2+}-free, high-K^+ PSS (composition below) were used in all experiments. Endothelial cells were loaded with the Ca^{2+} indicator dye Cal-520/AM (5 μM in PSS + 0.02% Pluronic F-127, 30 min, 37°C) and then mounted in a custom flow chamber (Wilson, Lee, & McCarron, 2016).

2.3 | Image acquisition

Four imaging systems were used:-

- *Imaging system 1*: a Nikon Eclipse TE300 inverted microscope fitted with a CoolLED pE-300 LED illumination system (490- and 550-nm excitation) and custom designed, dual fluorescein isothiocyanate/tetramethylrhodamine (FITC/TRITC) filter sets (Figure S1A). A 40× 1.3 NA Nikon S Fluor oil-immersion objective lens was used for Ca^{2+} imaging experiments and a 100× 1.3NA Nikon S-Fluor lens for imaging immunocytochemistry endothelial patches. Images were acquired using an Andor iXon EMCCD camera (1024 × 1024).
- *Imaging system 2*: a Nikon Eclipse FNI upright microscope equipped with a Nikon Fluor 16× 0.8 numerical aperture (NA) water immersion and a pE-4000 CoolLED system (490 and 550 nm) and a custom designed dual FITC/TRITC filter set (Figure 3a(ii)). Images were acquired using an Andor iXon EMCCD camera (1024 × 1024). This system was used for experiments involving focal puffer application of drugs with simultaneous global flow.
- *Imaging system 3*: a Nikon Eclipse FNI upright microscope equipped with a Nikon Fluor 16× 0.8 NA or 40× 0.8 NA water immersion objective lens and a pE-4000 CoolLED system (490 and 550 nm) and a custom designed dual FITC/TRITC filter set (Figure 5a(i)). Images were acquired using a Photometrics Evolve 13 EMCCD camera (1024 × 1024). This system was used for (1) contraction and relaxation experiments, (2) for experiments involving focal puffer application of drugs simultaneously with photo-uncaging, (3) photo-uncaging and (4) fluorescence recovery after photobleaching (FRAP) experiments. All images were acquired using MicroManager v1.4.22.
- *Imaging system 4*: a Nikon FNI upright microscope with an Aurox Clarity box between the camera and the microscope optics to provide structured illumination and a spinning disk for confocal imaging. A PCO Edge 5.5 EMCCD was used for image acquisition. A Nikon 60× water 1.0NA lens was used for image acquisition in Micromanager v2.0. This system was used for imaging immunocytochemistry results in intact arteries.

2.4 | Localized uncaging

1. In experiments in which endothelial Ca^{2+} responses were evoked by photolysis of caged IP_3, the endothelium was loaded with Cal-520/AM, 0.02% Pluronic F-127 and a membrane-permeant Ins (1,4,5)P3-caged IP_3 (5 μM; cIP_3; 30 min at 37°C) (Buckley et al., 2020, 2021). In experiments using localized Ca^{2+} buffering, the caged Ca^{2+} buffer membrane-permeant Diazo-2/AM (McCarron et al., 2010) (5 μM, 30 min at 37°C; kindly provided by Prof Alexi Tepikin) was also loaded into cells. When using Diazo-2, the dye was

constantly kept in the dark, even when dissolving the desiccated powder in DMSO. In caged Ca^{2+} experiments, the endothelium was dual loaded with Cal-520/AM and membrane-permeant nitrophenyl (NP)-ethylene glycol tetra-acetic acid (EGTA)/ acetoxymethyl ester (AM) dye (5 μM; Invitrogen: 30 min at 37°C). When using NPEcIP3 (5 μM), a non-membrane permeant form of caged IP_3, the dye was added to the bath and a recording performed immediately.

Two photolysis systems were used. Photolysis of cIP_3 on imaging system 3 was achieved using a Rapp OptoElectronic DL-Series UV (375 nm) laser coupled into a Firefly system, with a UGA-42 scanner, to permit the uncaging region to be set via software. The UV photolysis light was first passed through an attenuating neutral density filter (1% transmission) and used at a power such that it was 2 mW before loss as it travelled through the optics.

Photolysis of cIP_3, Diazo-2 or NP-EGTA on imaging system 1 was achieved using a Rapp Optoelectronics flash lamp (00-325-JML-C2) at 200 V, which produced light of ~1-ms duration (Buckley et al., 2020; McCarron et al., 2000). The flashlamp output was passed through a 395-nm short pass filter into a 1250-μm diameter light guide. The light guide was coupled to the epi-illuminator of the TE300 microscope and the output focused onto the endothelium using broadband light. For each imaging session, broadband light was used to identify the position of the uncaging region (~70-μm diameter) and determine which endothelial cells were directly activated by the spot photolysis system.

cIP_3-evoked endothelial Ca^{2+} activity was imaged at 10 Hz. Baseline Ca^{2+} activity was recorded for 30 s and then endothelial Ca^{2+} activity was evoked by photolysis of cIP_3. All cIP_3 uncaging experiments were performed with 15-min rest between each photolysis event to allow for Ca^{2+} store refilling. For Diazo-2 experiments, Ca^{2+} activity was recorded at 10 Hz and Diazo-2 uncaged after 30 s. For NP-EGTA experiments, Ca^{2+} activity was recorded at 10 Hz and uncaging performed every ~10 s.

2.5 | Fluorescent recovery after photobleaching (FRAP)

Preparations were loaded with the cell-permeant fluorophore calcein/AM (0.02% Pluronic F-127, 30 min, 37°C). FRAP experiments were performed on imaging system 3 using a ROE DL-Series UV (375 nm) with a UGA-42 scanner. The FRAP region was selected via the controlling software. A 40× 0.8NA water-immersion lens was used and the power measured at approximately 8 mW. The scan was repeated approximately five to 10 times to reduce the fluorescence intensity within the FRAP region to ~70% of the initial value. Images were then acquired at 0.1 Hz for 1 h to image the recovery period.

2.6 | Immunocytochemistry

The Immuno-related procedures used comply with the recommendations made by the *British Journal of Pharmacology* (Alexander et al., 2018). Freshly isolated endothelial cell patches or *en face* arterial preparations were fixed in 4% paraformaldehyde (PFA; Agar Scientific, UK) in phosphate buffered saline (PBS) (20 min, room temperature), refreshing the PFA after 10 min. Cells were then washed (5 min) three times in glycine solution (0.1 M), then three times in PBS (5 min) and then permeabilized with Triton-X100 (0.2% in PBS; 30 min). Cells were washed three times in PBS (5 min), then three times in an antibody wash solution (0.15 M NaCl, 15-mM Na3C6H5O7, 0.05% Triton-X100 in Milli-Q water; 5 min), and incubated with blocking solution (5% donkey serum in antibody wash solution; 1 h at room temperature). Cells were incubated overnight at 4°C with an anti-CD31 (PECAM) primary antibody (R&D Systems cat. # AF3628, RRID:AB_2161028, 1:1000, raised in goat) and either an anti-IP_3R (Millipore, Cat. # 07-1210, RRID:AB_1587207, 1:100, raised in rabbit), anti-Cx43 (Sigma Aldrich Cat. # C6219, RRID:AB_476857, 1:400, raised in rabbit), anti-**$P2Y_2$** receptor (Alomone Labs, Cat. # APR-010, RRID:AB_2040078, 1:1000, raised in rabbit), Anti-Panx1 (Alomone Labs, Cat. # ACC-234, RRID:AB_2340917, 1:1000, raised in rabbit) primary antibody, each diluted in antibody buffer at the concentrations stated (0.15 M NaCl, 15-mM $Na_3C_6H_5O_7$, 2% donkey serum, 1% BSA, 0.05% Triton X-100 and 0.02% sodium azide in Milli-Q water). All antibodies were used only once. Cells were washed three times in antibody wash solution (5 min) and incubated with fluorescent secondary antibodies conjugated to Alexa Fluor 488 (donkey anti-goat, Thermo Fisher Scientific Cat. # A-11055, RRID:AB_2534102, 1:1000 for the PECAM) and Alexa Fluor 555 (donkey anti-rabbit, Thermo Fisher Scientific Cat. # A-31572, RRID:AB_162543, 1:1000 for the other antibodies) in antibody buffer (1 h at room temperature). Cells were washed three times in antibody wash solution, incubated with the nuclear stain, **4′,6-diamidino-2-phenylindole (DAPI**; 4 nM; 5 min) and finally washed three more times in PBS (5 min) prior to imaging. Images were acquired either using (endothelial patches) a 100× lens on imaging system 1, or (*en face* arterial preparations) a 60× 1.0 NA water dipping lens on imaging system 4; 5% LED light was used with 100- to 500-ms exposure, high signal optical sectioning, 1-μm axial step size and a maximum intensity projection performed for image presentation.

2.7 | Electron microscopy

Arteries were pinned out in an *en face* configuration on Sylgard blocks. Blocks with mounted arteries were then transferred to 4% PFA (paraformaldehyde)/2.5% glutaraldehyde in 0.1 M phosphate buffer (72-mM $Na_2HPO_4.2H_2O$, 28-mM $NaH_2PO_4.2H_2O$ in Milli-Q water, pH 7.2) for 4 h at room temperature, then stored in 1:10 solution at 4°C prior to processing. Processing was carried out in a Pelco Biowave Pro+ at the University of Aberdeen. Arteries were washed in 100-mM cacodylate buffer followed by secondary fixation and heavy metal staining with 1% OsO_4 and 0.5% $K_3Fe(CN)_6$. Arteries were then washed with Milli-Q water followed by dehydration with ethanol (50%, 70%, 95%) then acetone prior to gradual infiltration of Spurr's resin (TAAB, UK) (10%, 30%,

50%, 70%, 90% in acetone). After infiltration was completed, sections were cut from the Sylgard blocks and embedded.

The resin was polymerized in a 60°C oven for 24 h. Sections (250 nm) were cut using a Leica UC6 ultramicrotome and Diatome diamond knife and collected on 100 square mesh grids and counterstained with Uranyless (TAAB, UK) and Ultrostain 2 (Leica, UK) using a Leica AC20. Tomograms were acquired on a Jeol 1400+ with AMT UltraVUE camera.

2.8 | Experimental protocols

In several experiments, directional flow of bath PSS was used to limit the spread of activators or inhibitors that were pressure ejected from a puffer pipette (puffer solution). Sulforhodamine B was included in the puffer pipette solution to visualize the location of ejected puffer solutions.

In those experiments that examined the propagation of Ca^{2+} signals elicited by application of **acetylcholine (ACh)**, ionomycin, IP_3 or PSS alone, endothelial Ca^{2+} activity was measured in the fluorescein isothiocyanate (FITC) channel and sulforhodamine was imaged in the TRITC channel. Images were acquired from alternating channels at 1 Hz per channel on imaging system 2 with a 16× water immersion lens. Directional PSS flow (1.5 ml·min^{-1}) was maintained along the artery throughout the experiment. ACh (50 nM or 100 nM) was added as indicated. In these experiments, ACh (1 μM) and sulforhodamine B (1 μM) or ionomycin (10 μM) and sulforhodamine B (1 μM) were focally applied by hydrostatic pressure ejection (Pneumatic PicoPump PV820, World Precision Instruments, Sarasota, FL, USA) from a puffer pipette (10 s) that was positioned perpendicular to the direction of PSS flow. Baseline Ca^{2+} activity was recorded for ~1.5 min before activation. When ionomycin had been applied to the endothelium, no subsequent experiments took place on that tissue.

In experiments using the **PLC** inhibitor **U73122**, preparations were incubated in cIP_3 (5 μM) and Cal-520 (5 μM) for 30 min at 37°C, and experiments were all performed on imaging system 3. In control experiments, uncaging was performed in the centre of the field-of-view (FoV) after a baseline recording (30 s). The entire preparation was then incubated in U73122 (10 μM) for 15 min and the uncaging repeated. In other experiments, in which U73122 was applied to restricted parts of the endothelium, the preparation was under PSS flow (1.5 ml·min^{-1} along the artery) throughout the experiment. A control uncaging was performed, after which a puffer pipette containing U73122 (10 μM) and sulforhodamine B (1 μM) was brought 30–60 μm from the endothelial surface and the puffer solution focally applied to one edge of the uncaging region for 15 min. A subsequent uncaging was then performed in the same central location as the control.

Experiments examining propagated vasodilation were performed on imaging system 3 using a 16× 0.8NA water immersion lens. Arteries were pre-constricted with **phenylephrine** (PE, 1–5 μM) and kept under a constant phenylephrine flow of 1.5 ml·min^{-1} throughout the experiment. A control cIP_3 uncaging across the upstream short axis of the preparation was performed and the ensuing vasodilation recorded until the artery relaxed fully and then re-constricted. Using pressure ejection, U73122 (10 μM) and sulforhodamine B (1 μM) were simultaneously applied focally to the region immediately downstream to the uncaging region for 15 min, after which a second uncaging was performed at the same site at which the control uncaging occurred. Images in the TRITC channel were acquired at 10 Hz throughout the experiment to determine the location of U73122.

U73122 has previously been shown to inhibit IP_3-evoked Ca^{2+} release by blocking IP_3R directly (MacMillan & McCarron, 2010). Those experiments used **U73122** from Tocris (Cat. # 1268) and the channel blocker was dissolved in chloroform, the solvent evaporated with nitrogen, then dissolved in DMSO. The current set of experiments used U73122 hydrate from Sigma (Cat # U6756), which is soluble in DMSO. This version of U73122, when used at 10 μM for 15 min, does not inhibit IP_3R directly. Control data, showing the absence of direct block, is shown in each relevant figure.

Where drugs such as apyrase (4 U·ml^{-1}) and **18α-glycyrrhetinic acid** (20 μM) were used, a control recording of cIP_3-induced wave propagation was taken after 30-s baseline recording and then the preparation rested for 15 min in PSS. The drug was then added and, after a 5-min incubation, the first recording taken. This was repeated every 15 min until four subsequent recordings had been taken. The preparation was incubated in the drug throughout. These experiments were performed using a 40× 1.4NA oil immersion lens on imaging system 1. A similar protocol was applied to the **LY294002** (300 μM)/**wortmannin** (50 μM) cocktail incubation on imaging system 3. In this case, each timepoint was acquired from a different artery that was taken from the same animal and pinned out in the same bath. Four initial control uncaging events were recorded at different sides and these same sites used for the final uncaging event.

When **cyclopiazonic acid** (CPA; 10 μM) was used, a control uncaging was first performed, the preparation was left to rest for 15 min in PSS, then cyclopiazonic acid in PSS was flowed in for 5 min while a recording was taken at 2 Hz. When the Cal-520/AM fluorescence level had plateaued, a final recording was taken at 10 Hz with an uncaging event performed after 30 s.

2.8.1 | The SPEAR (SPecific Endothelial Area Removal) technique

Cell–cell contact was disrupted in the intact endothelium to create a gap between cells (discontinuity). In these experiments, an initial control uncaging (after 30s baseline recording) was first performed and wave propagation determined. A heavily heat polished (rounded) pipette was then used to precisely remove a strip of endothelial cells across the entire vessel to create a gap of ~50 μm between cells on each side of the discontinuity. The preparation was left to rest for 15 min, after which a second uncaging was performed to visualize Ca^{2+} wave propagation towards and beyond the discontinuity. Uncaging was then repeated in the absence (control) or presence of either global or localized flow. In a subset of experiments, the ATP receptor blockers, **suramin** (100 μM) or ARC118925XX and **MRS2179** (10 μM)

(each 45 min), were applied before the final cIP_3 uncaging. Propidium iodide (2.5 μM) was added at the start and end of the experiment to verify removal of cells and location of cell death. A UV LED (370 nm) was used to check the integrity of the internal elastic lamina. This technique was performed on imaging system 3 using a 16× 0.8NA water dipping lens.

2.9 | Membrane potential

The contribution of membrane potential changes to cIP_3-induced wave propagation was investigated. In these experiments a high-K^+/Ca^{2+}-free PSS (79.7-mM NaCl, 2-mM MOPS, 70-mM KCl, 1.2-mM NaH_2PO_4, 5-mM glucose, 0.02-mM EDTA, 2-mM NaPy, 1-mM MgC_2l, 1-mM EGTA) was used to prevent plasma membrane potential changes. The high-K^+ PSS was Ca^{2+}-free to prevent smooth muscle contraction. In these experiments, after cIP_3 uncaging in high-K^+/Ca^{2+}-free PSS, a period of 15 min was left between each activation, during which the bathing media was changed to normal PSS (for store refilling to occur). Normal PSS was then replaced with Ca^{2+}-free PSS and then high-K^+/Ca^{2+}-free PSS for the next cIP_3 uncaging to occur. These experiments were performed on imaging system 1 using a 40× 1.4NA oil immersion lens.

The membrane potential kit, FluoVolt, was used to assess membrane potential during wave propagation events. Preparations were incubated in Fluoolt (1:1000) with PowerLoad (1:100) for 5 min at room temperature, then washed thoroughly before use. While the incubation time in the manual states 30 min, in the present experiments a maximum of 3 min was found to best stain endothelial cell membranes and limit non-specific staining. These experiments were performed using a 100× oil immersion lens on imaging system 1.

2.10 | Ca^{2+} signal analysis

Ca^{2+} signals were measured in each cell as previously described (Wilson, Lee, & McCarron, 2016). In brief, automated Fiji macros were used to extract cell coordinates and track cell positions between datasets. Single-cell Ca^{2+} signals were then measured from each cell and processed using a custom algorithm written in the Python programming language (Wilson, Lee, & McCarron, 2016; Wilson, Saunter, et al., 2016a, 2016b). Raw fluorescence (F) signals were converted to baseline-corrected fluorescence intensity (F/F_0) by dividing each intensity measurement by the average value of a 100-frame baseline period at the start of each trace. F/F_0 signals were smoothed using a 21-point third order polynomial Savitzky–Golay filter and key signal parameters (e.g. amplitude, frequency, number of cells and time of event) extracted automatically. Analyses of cIP_3-evoked Ca^{2+} responses were performed either within the photolysis region, or for the entire FoV. Analysis in the uncaging region of interest (RoI) was performed by applying a mask restricted to the photolysis region, determined using the image acquired when the flash lamp or laser was running. All activated cell numbers refer to the entire FoV.

To visualize Ca^{2+} wave propagation, images of active Ca^{2+} wavefronts were created by calculating $\Delta F/F_0$ for each image in the recording, or by using a sequential subtraction of images. For cIP_3-evoked Ca^{2+} experiments, a maximum intensity projection of the first 2 s (20 frames) immediately following uncaging was taken and presented using a JET LUT. Because experiments were paired (unless otherwise stated), images were contrast matched for control and treatment.

Analysis of signal propagation in puffing experiments was performed in MATLAB R2018b using custom written code. In these experiments, the fluororphore sulforhodamine B (1 μM) was included in the puffer pipette together with either ACh or ionomycin. Sulforhodamine B was used to determine the site of activator application from the puffer pipette. Those signals that overlapped with sulforhodamine B were excluded (because this is the site of the activator). To limit the influence of random basal activity, Ca^{2+} signals occurring in cells more than 200 μm from the uncaging region were eliminated from the analysis. In experiments in which ionomycin was applied in the continued presence of ACh, signals below 0.2 $\Delta F/F_0$ (i.e. evoked by ACh alone) were eliminated. Finally, only cells exhibiting signals during the puffer activator application were counted in the analysis. The number of cells and the shortest distance from the activation RoI were calculated for cells that met these criteria.

2.11 | FRAP analysis

FRAP was performed in a region that encompassed approximately five cells. Fluorescence recovery was acquired at 0.1 Hz for 1 h. Fluorescence intensity from the FRAP region was calculated and normalized to the whole FoV fluorescence and FRAP area. The change in fluorescence (expressed as arbitrary fluorescence units; AFU) between the first recording post-FRAP and the final recording was calculated, and the percentage intensity change calculated over 1 h.

2.12 | Endothelial patch isolation

First- to fourth-order mesenteric artery segments were dissected, cleaned of fat, cut open and the blood removed. Arteries were then cut into six strips of approximately 2-mm length and enzymatically digested using collagenase (Type 2, 256 units·mg^{-1}, 2 mg·ml^{-1}) in a water bath at 37°C for 35 min. The supernatant was then removed gently and the endothelial cell patches isolated by tituration using a wide-bored, fire-polished glass pipette. Patches were transferred to a glass-bottomed imaging chamber for Ca^{2+} imaging, or an eight-well chamber slide (μ-slides; Ibidi, Germany) for immunocytochemistry.

2.13 | Data and statistical analysis

The data and statistical analysis comply with the recommendations on experimental design and analysis in pharmacology (Curtis et al., 2018).

Summarized data are presented as means ± standard deviation values; n always refers to the number of animals. Matched experiments are indicated graphically by lines linking data points, unless otherwise stated. Data were compared as indicated using a two-tailed Student's *t* test (paired data) or a two-tailed one-way ANOVA with Sidak's or Tukey's multiple comparisons test, as appropriate. A post-hoc test was only performed if *F* was significant and there was no variance inhomogeneity. All statistical analyses were performed using GraphPad Prism, version 6.0 (GraphPad Software). A *P* value <0.05 was accepted as statistically significant. All tests, n numbers and significance values are noted in the figure legends.

2.14 | Materials

Cal-520/AM was obtained from Abcam. Pluronic F-127, NP-EGTA/AM, calcein/AM, donkey anti-rabbit 555 secondary antibody, donkey anti-goat 488 secondary antibody and FluoVolt membrane potential dye were obtained from Invitrogen. Anti-Cx43 primary antibody, ionomycin, acetylcholine, NaCl, MOPS, KCl, NaH_2PO_4, glucose, EDTA, NaPy, MgCl, EGTA, U73122, apyrase, 18α-glycyrrhetinic acid, sulforhodamine B, phenylephrine, suramin, LY294002, wortmannin and cyclopiazonic acid were obtained from Sigma Aldrich. ARC118925XX and MRS2179 were obtained from Tocris. Ins(1,4,5)P3-caged IP_3 was obtained from SiChem. D-myo-Inositol-1,-4,5-triphosphate (sodium salt; IP_3) was obtained from Cayman Chemical Company. All solutions were prepared fresh each day.

Details of other materials and suppliers are provided in the specific sections.

2.15 | Nomenclature of targets and ligands

Key protein targets and ligands in this article are hyperlinked to corresponding entries in the IUPHAR/BPS Guide to PHARMACOLOGY http://guidetopharmacology.org and are permanently archived in the Concise Guide to Pharmacology (Alexander, Kelly, et al., 2023; Alexander, Christopoulos, et al., 2023; Alexander, Mathie, et al., 2023; Alexander, Fabbro et al., 2023).

3 | RESULTS

In endothelial cells, in an intact artery, local photolysis of caged IP_3 (cIP_3) evoked a rapid rise in Ca^{2+} in the photolysis site, which subsequently propagated approximately concentrically outwards from the uncaging region (Figure 1a, Video S1). The propagated Ca^{2+} activity, visualized using the Ca^{2+} indicator Cal-520/AM, has been overlaid onto the endothelial field, alongside the time of each cell's activation after uncaging (Figure 1a). The increase in Ca^{2+} evoked by cIP_3 was reproducible (Video S1; Figure S2A–C) and abolished by store depletion using cyclopiazonic acid (Figure S2D). In controls, the average Ca^{2+} response, the area of signal propagation, the signal propagation speed and number of cells activated were each unchanged across multiple uncaging repeats (Figure S2A–C).

In a first series of experiments to examine intercellular communication, Ca^{2+} concentration was visualized individually in ~1000 endothelial cells while focally activating a preselected group of ~90 cells by cIP_3 (Figure 1b). When cIP_3 was locally uncaged, the propagating Ca^{2+} signal did not alter vessel tone (Figure 1b(i–iii)). When arteries were contracted with phenylephrine (PE, 1 μM, added to PSS flow; Figure 1c), focal uncaging of cIP_3 also evoked a robust outwardly propagating Ca^{2+} wave. The PE-contracted artery responded to the propagating Ca^{2+} wave with a relaxation (vasodilation) that propagated far beyond the uncaging region (Figure 1c). The vasodilation occurred more slowly and was more persistent than the propagating Ca^{2+} wave (Figure 1c). These data show that the mechanisms driving Ca^{2+} wave propagation are important for endothelium-dependent propagated vasodilation and maintenance of vessel tone.

3.1 | The role of Ca^{2+} and IP_3 in endothelial Ca^{2+} wave propagation

The propagated Ca^{2+} signals arise from cell–cell communication because no cIP_3 uncaging occurred outside the photolysis site (Figure S1). The mechanisms responsible for Ca^{2+} wave propagation may involve diffusion of IP_3 or Ca^{2+} (or both), via gap junctions or other communication junctions. In a first step towards determining the mechanisms, the role of Ca^{2+} in wave propagation was examined.

To do this, spatially and temporally localized Ca^{2+} buffering was used to selectively prevent the Ca^{2+} rise, triggered by uncaged cIP_3, in the photolysis site alone. This was achieved by photo-release of the photoactivatable Ca^{2+} buffer Diazo-2/AM (kindly provided by Prof Alexi Tepikin). When cIP_3 was uncaged in controls (i.e. in the absence of Diazo-2), a clear outward Ca^{2+} wave occurred (Figure 2a). The same preparations were subsequently loaded with Diazo-2/AM. Simultaneous photo-release of cIP_3 and Diazo-2 failed to generate a Ca^{2+} rise in the photolysis region. However, remarkably, an outwardly propagating Ca^{2+} wave still occurred outside the uncaging region (Figure 2a). This result suggests that the stimulus for Ca^{2+} wave propagation is not the increase in Ca^{2+} triggered by IP_3 but IP_3 itself.

To verify these results, the experiment was performed in reverse. A rise in Ca^{2+} was generated selectively in a localized group of endothelial cells using NP-EGTA (o-Nitrophenyl EGTA), a photolabile chelator that exhibits high affinity for Ca^{2+} until exposed to UV illumination. Despite a marked rise in Ca^{2+} within the photo-uncaging region, no propagated intercellular Ca^{2+} wave occurred, even after progressively increased Ca^{2+} loads (Figure 2b).

In a further test for the role of Ca^{2+} in wave propagation, localized Ca^{2+} rises were evoked by focal application of Ca^{2+} mobilizing agents. Focal application by pressure ejection from a puffer pipette of, first, the muscarinic receptor agonist, acetylcholine (ACh, 1 μM) evoked an IP_3-mediated Ca^{2+} response (Figure 3a(i), upper panel). In

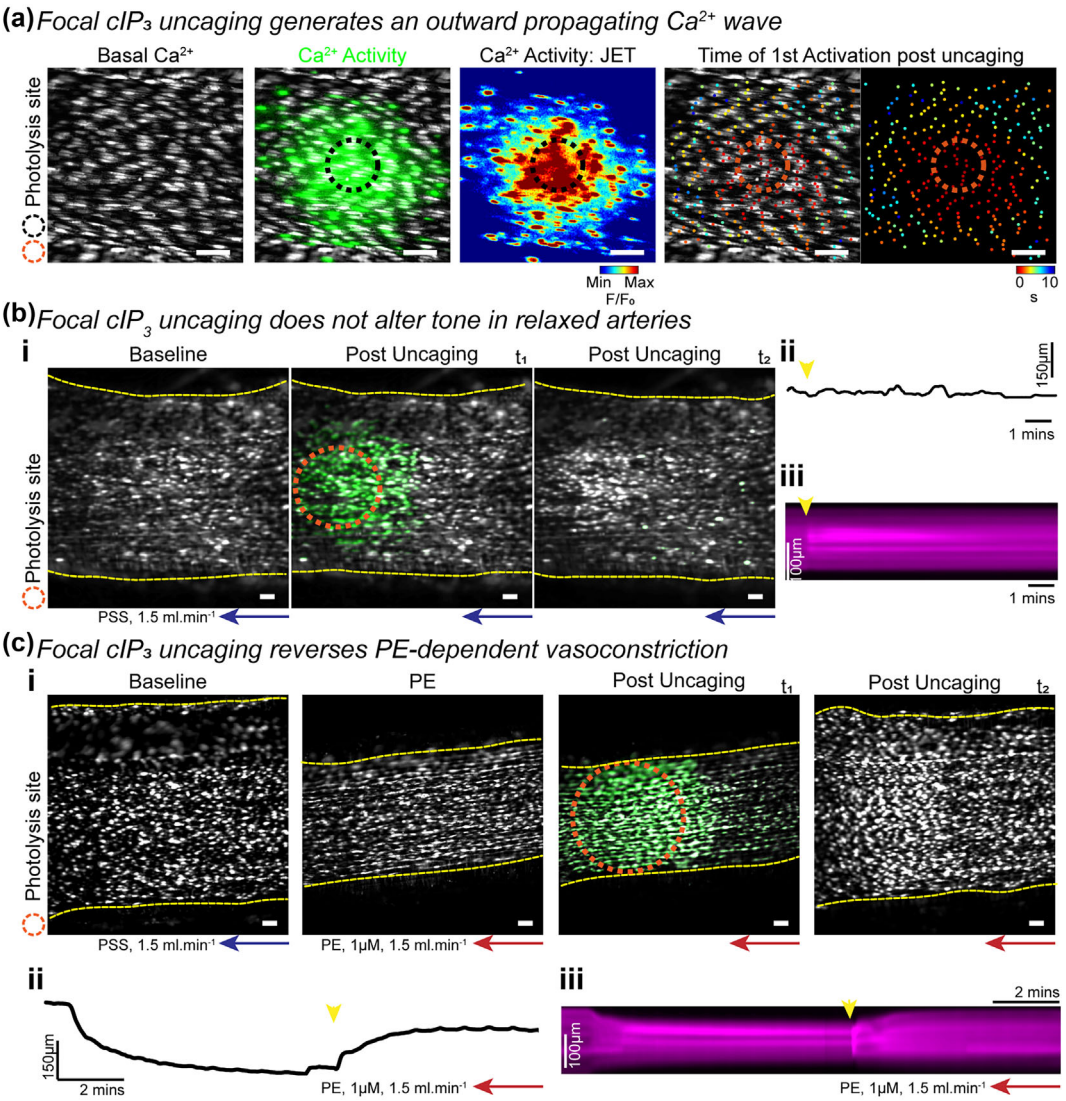

FIGURE 1 Localized cIP_3 uncaging in pre-constricted arteries causes endothelium-dependent vasodilation. (a) Representative image of endothelial cells in an *en face* preparation, loaded with Cal-520/AM (5 µM) and cIP_3 (5 µM). Basal Ca^{2+} signal (grey) and cIP_3-evoked Ca^{2+} activity (overlaid in green), acquired using imaging system 1 (see Section 2) are shown. Ca^{2+} activity (F/F_0) is also represented using the JET LUT; these representations are used throughout the paper. *Right-panel* cells are coded with the time the first measurable signal after cIP_3-uncaging occurs, shown here overlaid with and without basal Ca^{2+}. (b) PSS or (c) phenylephrine (PE; 1 µM) was delivered at a constant rate (1.5 ml·min^{-1}) using a continuous perfusion system (arrows indicate flow direction; blue bar (b): PSS; orange bar (c): PE). (i) Images of endothelial cells at baseline, after stimulation of smooth muscle contraction using PE (1 µM, (c) only), at 10s (t_1) and 3 min (t_2) after photo-release of cIP_3. cIP_3 uncaging-evoked endothelial Ca^{2+} activity is overlaid in green. The yellow dashed line marks vessel edges; the orange dashed circle marks the location of localized photo-release of IP_3. cIP_3-evoked laser photolysis was performed using imaging system 3 (see Section 2) with counter propagating flow. (ii) Vessel diameter was calculated using Vasotracker (Lawton et al., 2019) and the profile plotted (ii). (iii) Kymograph plotted throughout the experiment showing diameter change. Yellow arrows indicated cIP_3 photolysis. All image scale bars = 50 µm.

the same region of cells, focal application of the Ca^{2+} ionophore, ionomycin (10 µM) evoked a non-IP_3 mediated Ca^{2+} response (Figure 3a(i), lower panel). To precisely identify which cells were activated directly by ACh or ionomycin, the fluorophore sulforhodamine B was simultaneously ejected from the pipette to visualize the spread of the puffer solution (Figure 3a(ii)). The extent of diffusion of the activators was also restricted by directional PSS flow. ACh and ionomycin each generated robust Ca^{2+} responses in the activated cells. However, while cells activated by ACh generated a Ca^{2+} wave that propagated against the direction of PSS flow and away from the activated region of cells, the ionomycin-evoked Ca^{2+} signal did not propagate and remained confined to those cells directly activated by the ionophore (Figure 3a, Video S2).

However, we noted that in the presence of Diazo-2/AM, the overall signal in the propagating Ca^{2+} wave was reduced (Figure 2a). The signal reduction may have arisen simply from the presence of

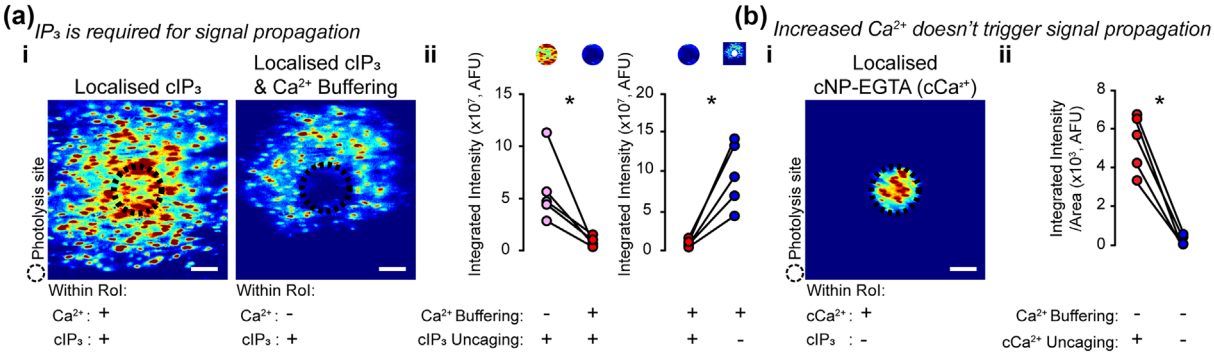

FIGURE 2 IP_3, not Ca^{2+}, is required for endothelial Ca^{2+} wave propagation. (a) (i) The endothelium was loaded with Cal-520/AM (5 μM) and cIP_3 (5 μM), and cIP_3 focally uncaged using imaging system 1 (see Section 2). In the left panel, photo-release of caged IP_3 (inside the black dotted line) evoked a Ca^{2+} increase that propagated outwards. Ca^{2+} activity (F/F_0) 2 s after uncaging is shown (JET LUT; blue low, red high Ca^{2+}). The right panel shows the same preparation after subsequent in situ loading with the photoactivable Ca^{2+} buffer Diazo/AM (5 μM). In the right panel, cIP_3 and Diazo-2 were simultaneously uncaged. No Ca^{2+} increase occurred in the photolysis site (black dotted line). However, Ca^{2+} increased outside the photolysis site. Ca^{2+} activity is again shown 2 s after uncaging (JET LUT, contrast matched with left panel). (ii) Summary data showing the Ca^{2+} change (integrated fluorescence intensity) inside the photolysis site after cIP_3 uncaging in the absence (pink circles) and presence (red circles) of Diazo-2 buffering, and within and outside the photolysis site in the presence of Diazo-2 buffering (n = 5). (b) The endothelium was loaded with Cal-520/AM (5 μM) and caged Ca^{2+} (NP-EGTA, 5 μM) and 20 flash photolysis events performed. The resulting Ca^{2+} activity (F/F_0) is shown (JET LUT). Summary data showing the Ca^{2+} change (integrated intensity/area) inside and outside the photolysis site (n = 5). All summary data are matched; * indicates statistical significance ($P < 0.05$) using a Student's *t* test. All image scale bars = 50 μm.

some uncleaved Diazo-2/AM in cells outside the photolysis site, resulting in an increased Ca^{2+} buffer capacity. However, it is also possible that Ca^{2+} was required alongside IP_3 to generate a robust Ca^{2+} wave.

To test for a facilitating role of Ca^{2+} in wave propagation, a localized (IP_3-independent) Ca^{2+} rise was evoked by ionomycin in the absence and presence of IP_3 generation by prior activation of the endothelium using ACh (50 nM or 100 nM; Figure 3b). Even with the endothelium preactivated with bath-applied ACh (Figure 3b(ii)), the Ca^{2+} rise generated by ionomycin did not evoke a propagating Ca^{2+} wave and the Ca^{2+} rise remained confined to those cells directly activated by the ionophore (Figure 3b). Taken together, these experiments show that (1) Ca^{2+} alone is not a major contributor to propagating Ca^{2+} waves in the endothelium and (2) IP_3 is critical for the generation of propagating Ca^{2+} waves.

3.2 | Regenerative IP_3 production drives Ca^{2+} wave propagation

We next asked: How does IP_3 act to drive Ca^{2+} wave propagation? The short half-time and range of action of IP_3 (e.g. ~1-s half-time with a range of action of 3 μm after photolysis of caged IP_3 in smooth muscle (Walker et al., 1987)) suggests that regenerative IP_3 production is required to account for wave transmission.

To test this hypothesis, a localized Ca^{2+} rise was evoked in endothelial cells by focal uncaging of cIP_3 in the absence and presence of the phospholipase C (PLC) inhibitor, U73122 (10 μM, 15 min; Figure 4a). PLC generates IP_3 by hydrolysis of phosphatidylinositol-4,-5-bisphosphate (PIP2). PLC inhibition with U73122 blocked cIP_3-generated wave propagation without altering the amplitude of the Ca^{2+} signal in the cells within the photolysis site (Figure 4a). We show that this is true in both males (Figure 4a(i)) and females (Figure 4a(ii)). This result suggests that local IP_3 release stimulates PLC activity in neighbouring cells to generate IP_3 production and propagate intercellular Ca^{2+} waves. To confirm this finding, U73122 was applied focally to a restricted population of cells on the outer edge of the photolysis site via pressure ejection of U73122 from a puffer pipette onto targeted cells (10 μM, 15 min; Figure 4b). A control uncaging of cIP_3 showed a clear outwardly propagating wave generated from the photolysis region. However, only those cells exposed to the PLC inhibitor did not show a Ca^{2+} increase in response to focal cIP_3 photolysis (Figure 4b, Video S3).

We validated this finding by blocking synthesis of the precursor to IP_3, **PIP2**, using the **phosphatidylinositol 4-kinase (PI4K)** inhibitors LY294002 (300 μM) and wortmannin (50 μM) (Balla et al., 2008; Harraz et al., 2018). An incubation time of 60 min effectively inhibited wave propagation and did not significantly change the Ca^{2+} response, though a slight reduction could be seen in some preparations (Figure 4c). These experiments demonstrate that IP_3 released in the photolysis site triggers regenerative IP_3 production that is required for wave propagation to occur.

We next addressed whether or not regenerative IP_3 production explained propagated vasodilation. Artery smooth muscle contraction was evoked using phenylephrine (PE; 1 μM) under constant flow and a localized cIP_3-driven rise in Ca^{2+} was used to elicit a propagated vasodilation (Figure 4d). After focal application of U73122 (10 μM, 15 min) downstream of the uncaging region and selectively to the endothelium, cIP_3-driven propagated vasodilation was significantly reduced in the PLC-blocked region (Figure 4d, Video S4). These data

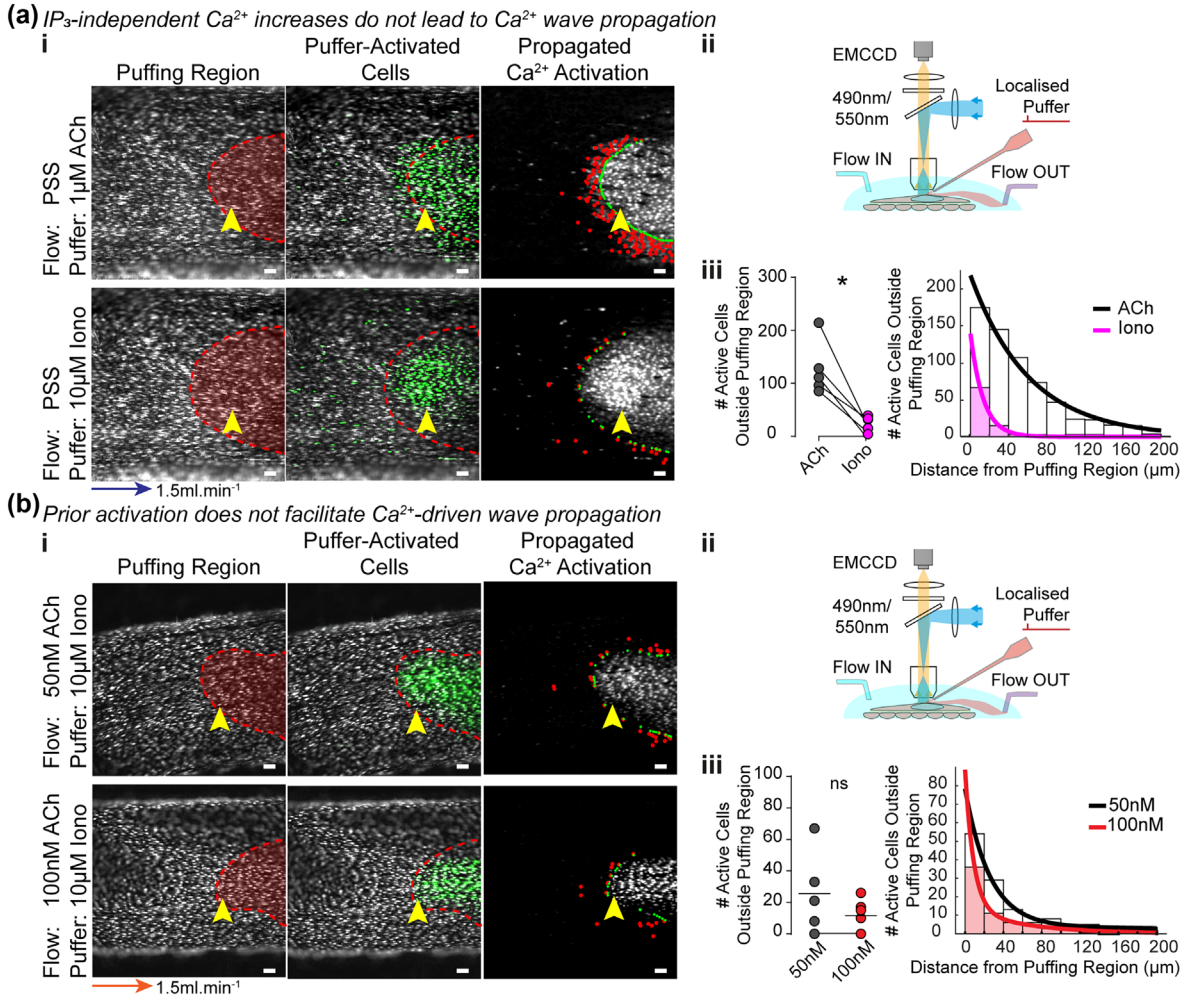

FIGURE 3 IP_3, rather than increased Ca^{2+} concentration, accounts for wave propagation. (a) (i) Representative fluorescence (Cal-520/AM signal) and puffer-induced Ca^{2+} activity (F/F_0; green overlay) images upon focal activation using (A) the muscarinic receptor activator ACh (1 μM; upper panel) then the Ca^{2+} ionophore ionomycin (10 μM; lower panel). Focally (puffer) applied ACh and ionomycin occurred either under PSS flow (A, blue arrow), or (b) ionomycin (10 μM) with ACh flow (orange arrow; 50 nM [upper panel] or 100 nM [lower panel]). Propagated Ca^{2+} activity (red points) and the puffing region edge (green points) are overlaid onto a greyscale image of total Ca^{2+} activity. The yellow arrow indicates the puffer pipette location and direction. (ii) Schematic of imaging system 2 (see Section 2) with localized puffing and flow. Focal endothelial cell activation was achieved using local agonist application by pressure ejection from a puffer pipette against the direction of constant PSS flow (1.5 ml·min^{-1}). All puffer pipette solutions contained sulforhodamine B (1 μM) to identify the region of influence of the perfused agonist (red dashed region). (iii) Summary data showing the extent of propagated Ca^{2+} activity after activation with ACh or ionomycin. Number of activated cells outside the puffing region with distance from the puffing edge is shown. Summary data (a(iii)) are matched (n = 5). Summary data from (b(iii)) are separate arteries because of the initial use of ionomycin (n = 5). * indicates statistical significance ($P < 0.05$) using a Student's *t* test. All image scale bars = 50 μm.

show that IP_3-mediated IP_3 production drives propagated vasodilation in intact mesenteric arteries.

3.3 | Gap junctions are not involved in endothelial Ca^{2+} wave propagation

It is reported widely that transmission of Ca^{2+} waves is facilitated by gap junction coupling between neighbouring cells (Boitano et al., 1992; Figueroa et al., 2004; Saez et al., 2023). We therefore explored what role, if any, that gap junctions played in Ca^{2+} wave propagation. Immunocytochemistry on endothelial cell patches confirmed that Cx43 was present in the endothelial cell membranes and electron micrographs of the endothelium show structural features consistent with cell–cell communication junctions, such as tight junctions, peg and socket junctions, and sites of attachment (Figure S3A).

Further support for functional communication junctions was established by imaging the movement of fluorophores between cells. 'Fluorescence recovery after photobleaching' (FRAP) of the fluorophore calcein/AM ($MW_{calcein}$ = 620 Da; MW_{IP3} = 420 Da) was used to examine the movement of small molecules between cells. Diffusion

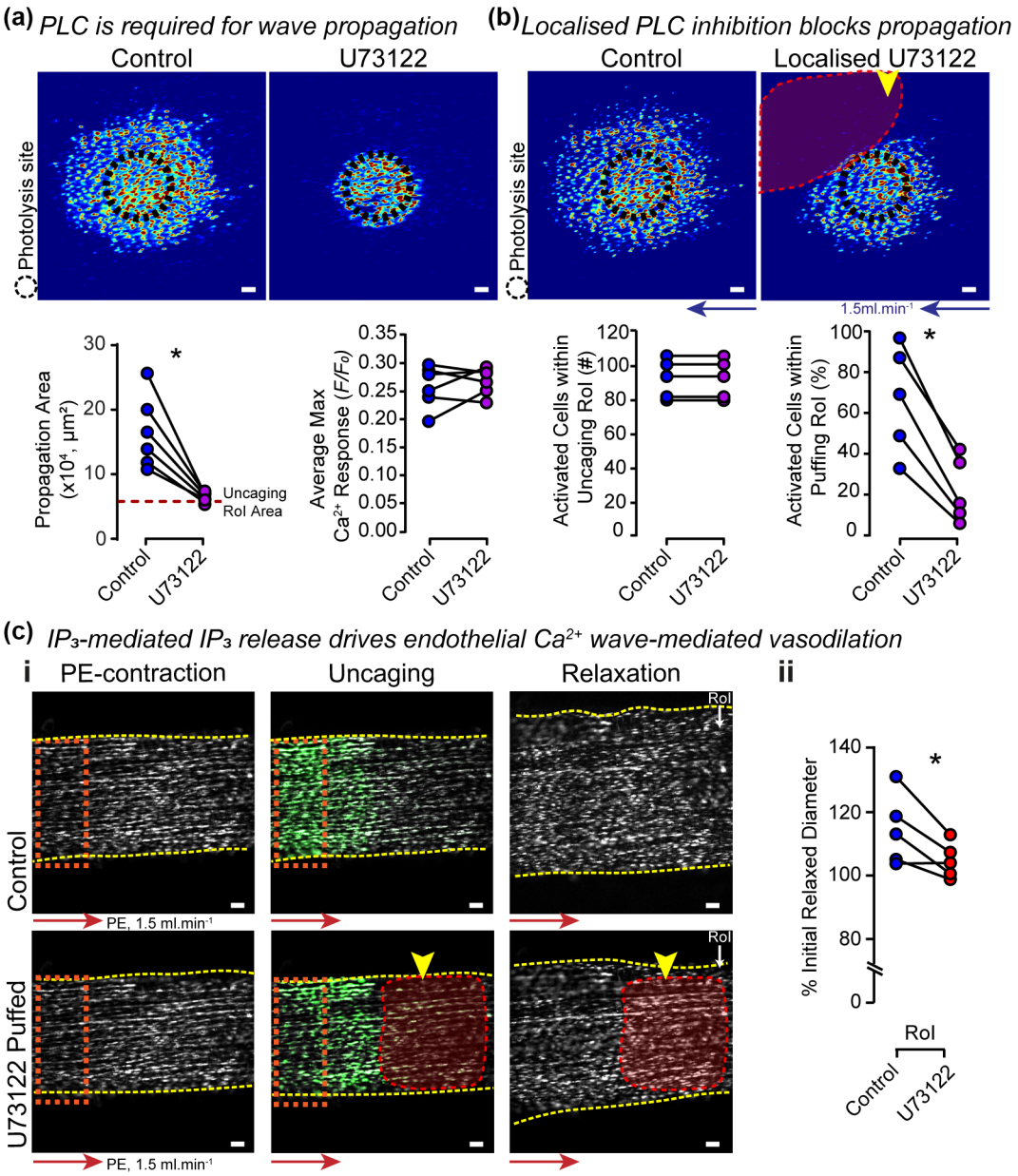

FIGURE 4 IP_3-mediated IP_3 production is required for endothelial Ca^{2+} wave propagation and propagated vasodilation. (a) Images, acquired on imaging system 3 (see Section 2), of cIP_3-generated Ca^{2+} activity (F/F_0) 2 s post uncaging (JET LUT, contrast matched), under control conditions and after PLC inhibition across the entire preparation using U73122 (10 µM, 15 min, right panel) in size-matched (i) male and (ii) female Sprague–Dawley rats. Summary data showing that blocking IP_3 generation with U73122 reduces the Ca^{2+} wave propagation area in males (n = 6) and females (n = 6) without reducing the initial Ca^{2+} release. (b) Images of cIP_3-generated Ca^{2+} activity (F/F_0) 2 s post uncaging (JET LUT, contrast matched) in the presence of counter-propagating PSS flow (1.5 ml·min^{-1}; blue arrow) alone or after focal U73122 (10 µM, 15 min, yellow arrow: puffer location) application using pressure ejection from a puffer pipette to a preselected endothelial region (right panel, red dashed region). Summary data showing focal inhibition of IP_3 generation with U73122 does not change the number of cells activated within the uncaging region, but significantly reduces the number of cells activated within the U73122 puffing region (n = 5). (c) Images of cIP_3-generated Ca^{2+} activity (F/F_0) 5 s post uncaging (JET LUT, contrast matched), in controls and after inhibition of PIP2 synthesis using a cocktail of LY294002 (300 µM) and wortmannin (50 µM) incubated for 60 min. Summary data showing that blocking PIP2 generation with LY294002 and wortmannin reduces the Ca^{2+} wave propagation area. The average Ca^{2+} response in the uncaging region was not significantly reduced, although a few preparations showed a decrease (n = 5). (d) (i) Phenylephrine (PE; 1 µM) was delivered at a constant rate (1.5 ml·min^{-1}; red arrow) to cause contraction. Images are shown prior to, during and after cIP_3-induced Ca^{2+} release (green overlay), either in controls or after focal application of U73122 (yellow arrow: puffer location, 10 µM, 15 min, red dashed region). The yellow dashed lines marks vessel edges; an orange dashed line marks the site of photo-released IP_3. (ii) Summary data showing that propagated vasodilation to the region of interest (RoI) does not occur where PLC has been focally inhibited by U73122 (n = 5). In all experiments that used a puffer for localized U73122 application, sulforhodamine B (1 µM) was included in the perfusion solution to accurately determine the area of U73122 action. Summary data are matched; * indicates statistical significance ($P < 0.05$) using a paired Student's *t* test. All image scale bars = 50 µm.

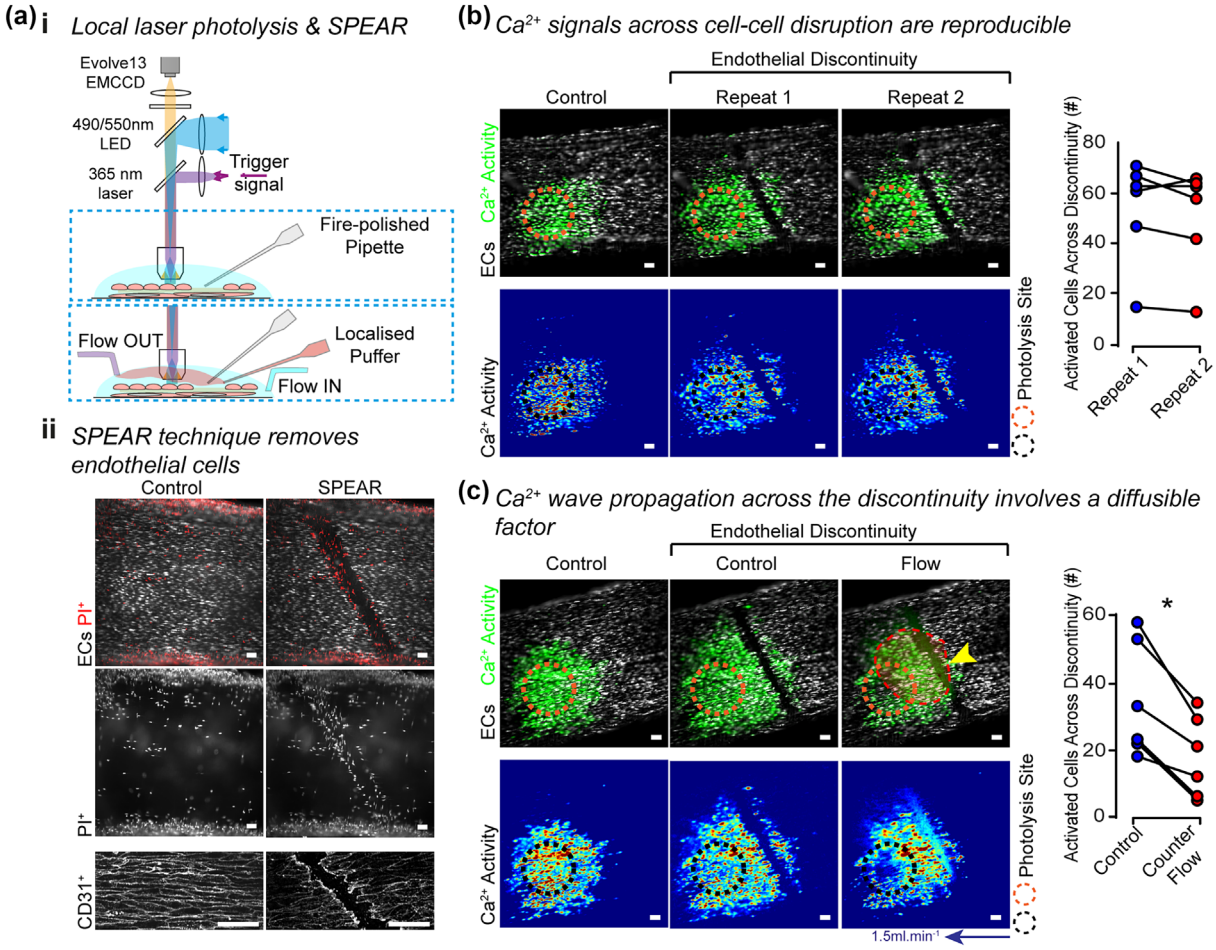

FIGURE 5 Reproducible Ca^{2+} wave propagation across endothelial discontinuities involves a diffusible factor. (a) (i) Schematic of imaging system 3 (see Section 2) with precision endothelial cell removal. Focal endothelial cell activation was achieved with a localized 365-nm laser. A pipette was heavily fire polished to melt and round the tip and was used to perform the SPEAR technique (see Section 2). (ii) Images taken on imaging system 3 (16× lens) of endothelial cells (grey) and propidium iodide staining (red, 2.5 μM) before (control) and after the introduction of a discontinuity using the SPEAR technique. Bottom panel: distinct arteries stained for CD31 (PECAM) without (control) or with (SPEAR) the introduction of a discontinuity (images taken on imaging system 4; maximum intensity projection, 60× lens). (b) Images of cIP_3-genereated Ca^{2+} activity (F/F_0) 10 s post uncaging (green and JET LUT, contrast matched) under control conditions and after two repeat uncaging events in the presence of an endothelial discontinuity. Summary data shows no significant difference in signal propagation across the endothelial discontinuity after two repeat uncaging events (n = 6). (c) Images of cIP_3-evoked Ca^{2+} activity (F/F_0; green and JET LUT, contrast matched) in the presence of global (blue arrow) and local (yellow arrow: location and direction of puffer pipette) PSS flow. Sulforhodamine B (1 μM) was included in the pipette solution to accurately show the area of PSS ejection (red dashed region). Summary data showing significantly reduced signal propagation across the endothelial discontinuity (n = 6). All summary data are matched; * indicates statistical significance ($P < 0.05$) using a paired Student's *t* test. All image scale bars = 50 μm.

of calcein to neighbouring cells after photobleaching did indeed take place. However, the rate of movement was significantly slower compared to the propagation speed of Ca^{2+} waves after localized uncaging of cIP_3 (Figure S3D). On average, full recovery after photobleaching required 100 ± 20 min. The speed of communication with cIP_3 uncaging and FRAP differed by several orders of magnitude (73 $\mu m \cdot s^{-1}$ vs. 0.014 $\mu m \cdot s^{-1}$, respectively). The slow spread of calcein after FRAP presumably reflects a limited permeability via communication junctions, perhaps because the junctions are largely closed.

To further investigate whether or not gap junctions play a role in Ca^{2+} wave propagation, 18α-glycyrrhetinic acid (18αGA, 20 μM, 50 min) was used to block gap junction function. Propagating Ca^{2+} waves were evoked using localized cIP_3 uncaging (Figure S3B). There was no change in the propagation area of the Ca^{2+} wave after 18αGA incubation (Figure S3B). We have previously shown that two commonly used gap junction blockers,18βGA and carbenoxolone, block IP3R activity, discounting them from being used to study the involvement of gap junctions on signal propagation (Buckley et al., 2021). It is therefore important to note that there was also no change in the IP_3-evoked Ca^{2+} response after incubation with 18αGA, showing that 18αGA does not block IP_3R activity.

To ensure that gap junctions were being blocked effectively by 18αGA at the concentration and incubation time used, FRAP experiments were performed. FRAP was seen in controls; however, it did

not occur in endothelial cells that had been preincubated in 18αGA (20 μM, 50 min; Figure S3C). This confirmed that while gap junctions were blocked, the cIP_3-generated Ca^{2+} wave was unaffected by 18αGA.

Taken together, these data suggest that, while gap junctions are present and functional in endothelial cells, communication through them happens on too slow a timescale to contribute significantly to Ca^{2+} wave propagation.

3.4 | Ca^{2+} waves occur independently of endothelial membrane potential

Changes in intracellular Ca^{2+} alter the plasma membrane potential in the endothelium. In some cells, changes in the plasma membrane potential may facilitate IP_3 production to generate IP_3-evoked Ca^{2+} release from intracellular stores (Mahaut-Smith et al., 1999). A link between membrane potential and IP_3 production could provide a regenerative mechanism to explain IP_3-mediated IP_3 release. To determine whether or not membrane potential changes were involved in IP_3-mediated IP_3 release, a localized uncaging of cIP_3 was evoked in high K^+ PSS, in which the membrane potential was held near the equilibrium potential for K^+ ($E_K \sim$ -18 mV). When compared to controls in normal PSS, there was no change in wave propagation, nor average Ca^{2+} response after photo-release of cIP_3 in high K^+ PSS (Figure S4A). This result suggests that hyperpolarization of endothelial cells is not required for the Ca^{2+} wave to propagate (Figure S4A). To ensure that high K^+ PSS did prevent endothelial hyperpolarization upon cIP_3 release, endothelial cells were loaded with a membrane potential indicator dye, FluoVolt and the change in fluorescence intensity imaged. As expected, hyperpolarization did not occur in high K^+ PSS (Figure S4B).

To test whether myoendothelial communication contributed towards IP_3-mediated IP_3 production-driven Ca^{2+} waves, freshly isolated endothelial cell patches were plated, stained with Cal-520 and cIP_3 and repeated photolysis applied to mirror the experiments performed in the intact arteries. Eliminating endothelial coupling with smooth muscle cells did not alter Ca^{2+} wave dynamics after photo-release of cIP_3 (Figure S4C). Reproducible Ca^{2+} waves were evoked that were indistinguishable from those seen in intact arteries (Figure S4C).

3.5 | Diffusible extracellular messengers propagate Ca^{2+} waves

In the absence of endothelial hyperpolarization or smooth muscle involvement, it is possible that an endothelial-released factor, such as ATP, that diffuses extracellularly could be a contributing factor to the propagation of Ca^{2+} waves (Ceriani et al., 2016; Kurth-Nelson et al., 2009). To test for a role of diffusible extracellular messengers in IP_3-mediated Ca^{2+} wave propagation, the structural proximity of neighbouring cells was disrupted to create a discontinuity in cell–cell contact (Video S5, Figure 6). If a diffusible messenger was involved, Ca^{2+} waves would propagate across a site in which there was no direct contact between cells. On the other hand, if cell–cell contact was required, the wave would terminate at the discontinuity (Cotrina et al., 1998; Gomes, Srinivas, Vereecke, & Himpens, 2005; Guthrie et al., 1999; Hassinger et al., 1996).

Cell–cell contact was disrupted, using the SPEAR technique (see Section 2), to approximately the length of a cell (~50 μm) using a fire polished pipette (Figure 5a(i), Video S5). Cell removal was confirmed using propidium iodide and CD31 (PECAM) immunolabelling (Figure 5a(ii)) and the integrity of the elastic lamina checked using UV illumination. The results show that Ca^{2+} waves, generated by photo-release of cIP_3, travelled reproducibly across discontinuities in cell–cell contact (Figure 5b).

To confirm that a diffusible factor contributed to signal transmission across the discontinuity, global and localized fluid flow was introduced against the direction of wave propagation (counter flow). Localized flow was achieved using a puffer pipette being brought to the outer edge of the discontinuity, just above the cell surface, and PSS with sulforhodamine B pressure ejected onto the preparation (Figure 5c). In the presence of counter flow, there was a significant reduction in signal propagation across the discontinuity (Figure 5c). This finding supports the suggestion of a diffusible messenger contributing to wave propagation. It should be noted that sulforhodamine B stained the elastic lamina, causing some (Ca^{2+} independent) fluorescence signal to occur within the discontinuity (Figure 5c).

The most obvious candidate for a diffusible factor was ATP. Therefore, the antagonist suramin (10 μM, 45 min) was used to block ATP P2 receptors (Figure 6a). Suramin significantly inhibited Ca^{2+} wave propagation across the discontinuity (Figure 6a(i)). Similarly, a significant reduction in signal propagation across the discontinuity occurred with the **$P2Y_2$ receptor** antagonist ARC118925XX and the **$P2Y_1$ receptor** antagonist MRS2179 (10 μM each, 45 min) (Figure 6a(ii)).

3.6 | Diffusible extracellular messengers do not propagate Ca^{2+} waves in intact preparations

The question now arises: Does ATP contribute as a diffusible messenger to Ca^{2+} wave propagation in the absence of a discontinuity? Under conditions lacking a distinct discontinuity, the propagation of Ca^{2+} waves was unaffected when ATP receptor activity was blocked using suramin (Figure 6b(i)) or ARC118925XX and MRS2179 (P2Yi; Figure 6b(ii)). Similarly, outward propagation was also unaffected in females in the presence of P2Yi (Figure 6c). Nor indeed was there any difference in propagation extent after incubation with apyrase (4 $U \cdot ml^{-1}$, 1 h), used to hydrolyse extracellular ATP (Figure S5A). These results suggest that ATP does not contribute to Ca^{2+} wave propagation when there is direct cell contact.

To further test whether any diffusible factor played a role in Ca^{2+} wave propagation in the absence of a discontinuity, rapid extracellular fluid flow was introduced across the intact preparation.

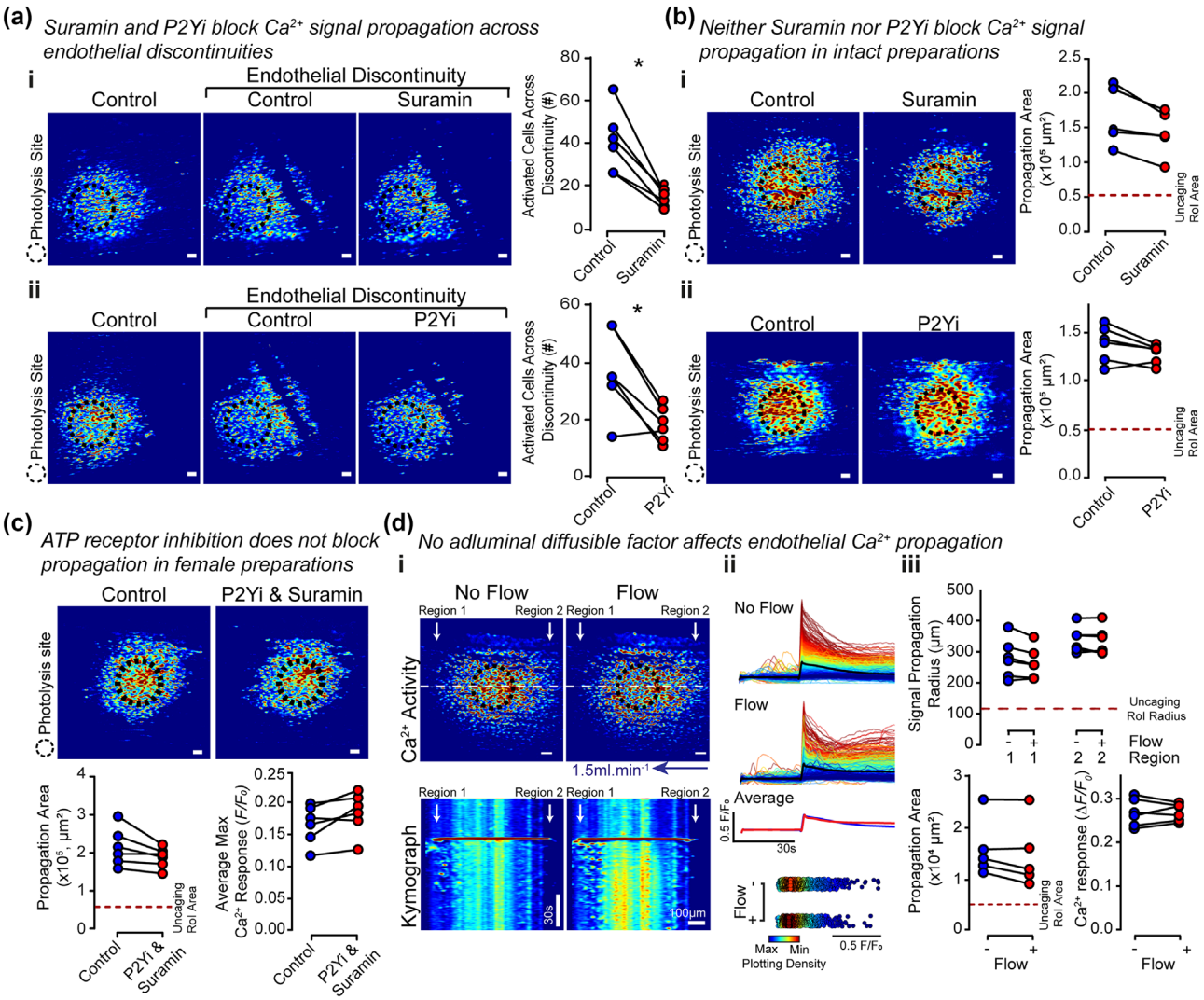

FIGURE 6 ATP drives Ca^{2+} wave propagation across endothelial discontinuities, but does not where there is cell–cell contact. (a) Images of cIP_3-genereated Ca^{2+} activity (F/F_0) 10-s post-uncaging (JET LUT, contrast matched) under control conditions, after a control uncaging event in the presence of an endothelial discontinuity and in the presence of (i) suramin (100 µM, 45 min) or (ii) $P2Y_1$ (i.e. ARC118925XX and MRS2179, 10 µM, 45 min). Summary data shows a significant decrease in signal propagation across the endothelial discontinuity in the presence of (i) suramin (n = 6) and (ii) $P2Y_1$ (n = 6). (b) Under the same experimental conditions, Ca^{2+} activity (F/F_0; JET LUT, contrast matched) and summary data show no change in propagation characteristics in intact preparations in the presence of either (i) suramin (n = 5) or (ii) $P2Y_1$ (n = 6) when there is no discontinuity. (c) Ca^{2+} activity (F/F_0; JET LUT, contrast matched) and summary data show no change in propagation characteristics nor Ca^{2+} response (n = 6) in intact preparations in the presence of suramin (100 µM) and $P2Y_1$ (ARC118925XX and MRS2179, 10 µM, 45 min) in intact preparations from weight-matched Sprague–Dawley female rats. (d) (i) Images of cIP_3-generated Ca^{2+} activity 10-s post-uncaging (F/F_0; JET LUT, contrast matched) are shown in the absence of flow (control) and with flow. A kymograph of the extent of propagation (x) over time (y) along the dashed white line is shown (JET LUT). (ii) F/F_0 signals for an individual dataset (no flow and flow) and their average signal overlaid. The maximum F/F_0 signal for each cell under each condition is plotted below. (iii) Summary data showing that the extent of outward propagation, the propagation area and the Ca^{2+} response (n = 6) are not significantly different in the absence and presence of flow. All image scale bars = 50 µm, unless individually stated. Summary data are matched; * indicates statistical significance ($P < 0.05$) using a paired Student's t test or a two way ANOVA.

If a diffusible messenger was involved, rapid fluid flow should introduce a bias to the direction of wave travel. cIP_3 was focally uncaged in the absence and presence of directional PSS flow (Figure 6d). No change in the Ca^{2+} response, the signal propagation radius on either side of the uncaging region, nor the propagation area, occurred in the presence of flow (Figure 6d). This result is consistent with other data in the intact preparation (i.e. absence of a discontinuity) already presented in this study using counter propagating flow and either cIP_3- or ACh-initiated IP_3-mediated Ca^{2+} waves (Figures 1, 2 and 4); directional flow did not alter Ca^{2+} wave characteristics. These experiments suggest that a diffusible messenger is an unlikely contributor to Ca^{2+} wave propagation in the intact preparation when there is direct cell contact (i.e. in the absence of a discontinuity).

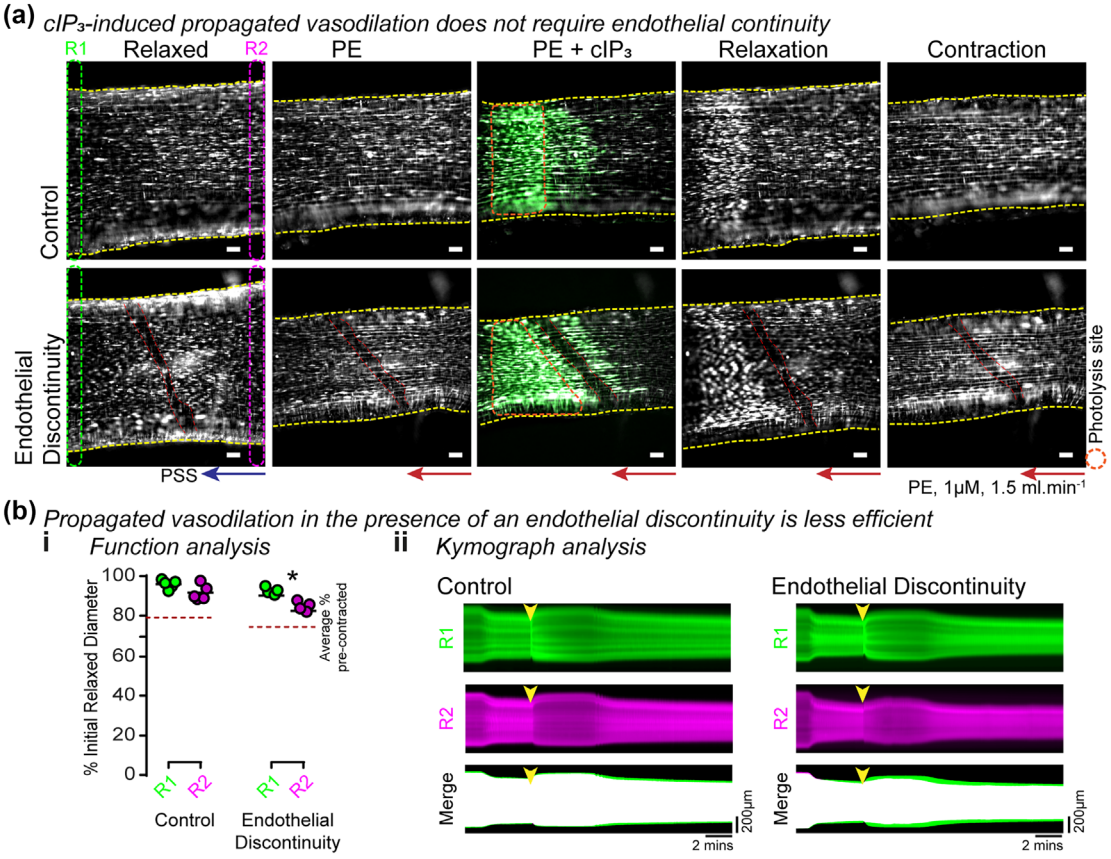

FIGURE 7 Propagated vasodilation still occurs in the presence of an endothelial discontinuity. (a) Mesenteric arteries were mounted on imaging system 3 (see Section 2). Focal endothelial cell activation was achieved with a localized 365-nm laser. A fire polished pipette was used to perform the SPEAR technique. Phenylephrine (PE; 1 μM) was delivered at a constant rate (1.5 ml·min^{-1}) using a continuous perfusion system (blue arrow: PSS; orange arrow: PE). After PE-induced contraction, a cIP_3 uncaging event was performed in either the control section or the section containing an endothelial discontinuity, triggering vasodilation and subsequent contraction recovery (vasoconstriction). Endothelial Ca^{2+} activity arising from cIP_3 uncaging is overlaid in green (F/F_0). Vessel edges are delineated using a yellow dashed line; an orange dashed line marks the location of localized photor-elease of IP_3. (b) (i) Summary data shows no change in vasorelaxation in R1, but a significant reduction in vasorelaxation in R2 ($n = 5$). (ii) Region 1 (green dashed box in a) and region 2 (magenta dashed box in a) were used to create a kymograph (representative examples shown) and the vasorelaxation calculated as a percentage of the initial relaxed diameter. Yellow arrows indicated cIP_3 photolysis on the kymograph. Image scale bars = 50 μm. A paired Student's *t* test was performed; $^*P < 0.05$.

The disparity between effective blocking of signal across a discontinuity by ATP receptor blockers, but with the same inhibitors showing no discernible effect on intact preparations, led us to hypothesize that signals could be travelling abluminally, such that flow and the luminal presence of P2Y receptor blockers and ATP inhibitors may have limited effect. To test this hypothesis, endothelial patches were isolated and Ca^{2+} wave propagation examined in the absence and presence of P2Y receptor inhibitors (Figure S5B). Again, no discernible effect was seen on wave propagation. Because the blockers would have free diffusion around the endothelial patch, this result suggests that ATP is an unlikely contributor to wave propagation when there is direct cell contact.

We next hypothesized that creating an endothelial discontinuity may have resulted in cell junctional pores being exposed where they would normally have been sealed between membranes. These exposed junctions could facilitate the release of ATP from cells. To assess this hypothesis, *en face* preparations were stained for the presence of Cx43 or Panx1, both reported to be involved in ATP release from endothelial cells (Filiberto et al., 2022; Gomes, Srinivas, Van Driessche, et al., 2005; Kang et al., 2008). These junctional proteins were indeed found to be co-localized with the membrane adherence protein PECAM at the site of the endothelial discontinuity (Figure S6). This route could provide a mechanism for ATP release at the discontinuity.

Together, these results suggest that two separate mechanisms permit Ca^{2+} signal propagation in the endothelium. Where there is direct cell–cell contact, IP_3-mediated IP_3 production accounts for intercellular Ca^{2+} wave propagation. In the absence of direct cell–cell contact, Ca^{2+} wave propagation is driven by ATP released as a diffusible extracellular messenger.

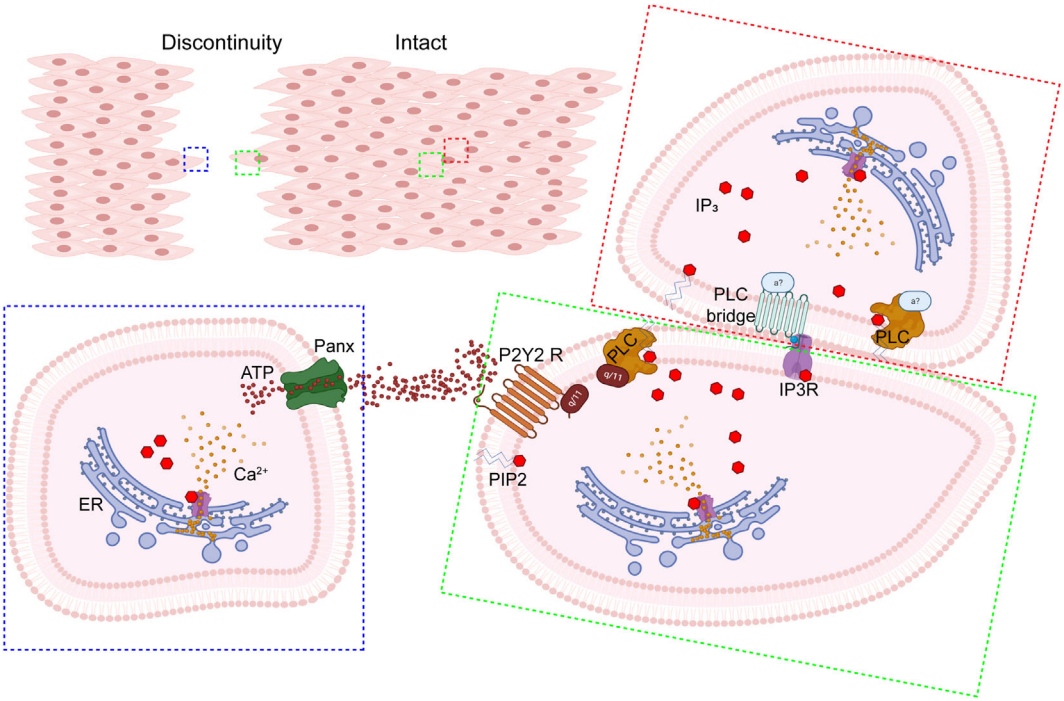

FIGURE 8 Summary of the signal switching used to maintain intercellular communication in the vascular endothelium. *Signalling where there is cell–cell contact:* IP_3 activates and IP_3R on the cell membrane (green box). This process initiates signal transduction that does not require the flux of Ca^{2+} or other molecules across the pore to initiate a signalling cascade. The signalling activates an unidentified 'PLC bridge' (red box) which could be a receptor such as a GPCR, an adhesion protein or some form of ligand. The PLC bridge either directly or indirectly activates phospholipase C (PLC) to mediate breakdown of PIP2, generate IP_3 and trigger Ca^{2+} release from ER. IP_3 activates IP_3-mediated IP_3 release in adjacent cells to regeneratively propagate the Ca^{2+} signal. *Signalling across a discontinuity*: Exposed endothelial cells, in which IP_3-triggered Ca^{2+} release is initiated, release ATP into the interendothelial discontinuity (blue box), most likely through Panx-1 channels. ATP then binds to surface $P2Y_2$ receptor on cells across the discontinuity to activate PLC, cleaving PIP_2 into IP_3. IP_3 then binds to IP_3R on the endoplasmic reticulum (ER) surface, causing Ca^{2+} release into the cytoplasm.

To verify that ATP-driven signal propagation across a discontinuity is extensive enough to effect functional change, propagated vasodilation was next examined in the absence or presence of an endothelial discontinuity (Figure 7a). Arteries were preconstricted with phenylephrine (1 μM, added to PSS flow) and cIP_3 uncaged locally in the endothelium. phenylephrine contracted arteries responded with a relaxation on photo-release of cIP_3 that propagated far from the uncaging region (Figure 7a, upper panel). The contractile state of the artery subsequently recovered. Next, cell–cell contact was disrupted by introducing an endothelial discontinuity in the same artery, using the SPEAR technique, and the endothelium again activated with photo-release of cIP_3. Once again, the artery responded with a relaxation that propagated far from the uncaging region (Figure 7a, lower panel). Thus, propagated Ca^{2+} signals and vasodilation each extended far from the uncaging region in either the absence or presence of an endothelial discontinuity. Despite showing a marked relaxation, the vasodilation was less pronounced beyond the endothelial discontinuity (Figure 7b). These results suggest that the endothelium contains a failsafe mechanism whereby signal propagation and functional activity is maintained, even in the presence of endothelial discontinuities.

4 | DISCUSSION

Intercellular signalling in the endothelium underlies the communication required to generate immune activity, modulate blood clotting and regulate the vasomotor responses underlying propagated vasodilation. One mechanism of communication that acts to coordinate cell activities, in tissue level responses, relies on the intercellular signalling mediated by the propagation of Ca^{2+} waves. Our results reveal that intercellular signalling switches maintain communication in the face of changing cell connectivity. When there is direct contact among cells, an increase in IP_3 is itself sufficient to evoke a regenerative phospholipase C-dependent, IP_3-induced IP_3 production that propagates across cells. While cell–cell contact is required for this form of communication, propagation occurs independently of gap junctions, membrane potential changes, Ca^{2+} release via the IP_3R or the release of extracellular messengers. However, when the adjacent structural proximity of cells is disrupted, communication is maintained by the release of extracellular messengers to transmit intercellular Ca^{2+} signals (Figure 8). These findings present a new view on the mechanisms underlying Ca^{2+} wave propagation with significant implications for cell–cell communication.

In support of regenerative IP_3 production over passive IP_3 diffusion, the published values for the half time of IP_3 in cells are too short to explain the extent and duration of wave progression. The half-time of IP_3 ranges from <100 ms in olfactory neuron microvilli (Breer et al., 1990) to ~1 s in smooth muscle (Walker et al., 1987) and Parotid acinar cells (Burgess et al., 1985), to ~9 s in neuroblastoma cells (Wang et al., 1995) and ~60 s in Xenopus oocytes (Sims & Allbritton, 1998). The effective distance of action of IP_3, derived from the half-time and diffusion coefficient of the inositide, ranges from ~300 to ~25 μm to <5 μm (Allbritton et al., 1992; Breer et al., 1990; Dickinson et al., 2016). While the brief measured half times of IP_3 permit rapid concentration adjustment when a stimulus is withdrawn, the values are largely incompatible with the duration (tens of seconds) and distances (mm) that waves propagate in the endothelium. The rapid half time of IP_3 suggests regenerative production of the inositide is required. This conclusion is supported by our results that show an inhibition of wave propagation by PLC and PIP2 inhibitors; IP_3 either directly or indirectly activates PLC in neighbouring cells. We also found that this mechanism was conserved across genders; wave propagation was suppressed in arterial preparations from female rats by a phospholipase C (PLC) blocker. Our results also show that extracellularly applied IP_3 did not elicit a Ca^{2+} response (Figure S7) suggesting the inositide acts intracellularly. Although IP_3 is the trigger, the mechanism whereby PLC activation in neighbouring cells occurs is unclear.

While IP_3R are best known as large-conductance cation channels, they do support additional cell functions that are separate from the Ca^{2+} release activity of the channel. For example, IP_3R activity triggers Ca^{2+} influx in staurosporine-induced cell death to promote caspase-3 activation in DT40-TKO cells (Khan et al., 2007). Channel-pore-dead mutants of IP_3R, in which Ca^{2+} could not permeate the channel, were still able to trigger staurosporine-induced Ca^{2+} influx across the plasma membrane. Staurosporine-induced Ca^{2+} influx was absent in IP_3R lacking its cytosolic C-terminal tail (Khan et al., 2007). IP_3Rs also facilitate interactions of active **STIM1 and Orai** to promote store-operated Ca^{2+} entry in a way that is also independent of Ca^{2+} release from the store (Chakraborty et al., 2022; Thillaiappan et al., 2019). This additional role for IP_3Rs is regulated by IP_3 but does not require a functional channel pore (Chakraborty et al., 2022). These findings reveal links between IP_3, IP_3Rs and Ca^{2+} signalling that are not mediated by the flux of Ca^{2+} across the channel (Chakraborty et al., 2022; Khan et al., 2007). Ion flux-independent functions of the IP_3R also include a structural role of receptor in linking the endoplasmic reticulum and mitochondria (Bartok et al., 2019). IP_3R may act as a scaffold or tether to hold mitochondria close to the endoplasmic reticulum. This structural role also persists in pore-dead IP_3R, indicating that Ca^{2+} release is not necessary to support these IP_3R-dependent structural organizations (Bartok et al., 2019).

In addition to IP_3R, several other ion channels have important signalling features that do not arise from the ion flux activities that are associated with the channels. Signalling functions that are independent of ion flux through the pore have been reported for **AMPA glutamate receptors** and **N-methyl D-aspartate receptors** (Dai et al., 2021), the kainate receptor (Rodríguez-Moreno & Lerma, 1998), the **nicotinic acetylcholine receptor** (Zakrzewicz et al., 2017), the **Kv1.3 potassium channel** (Jiménez-Pérez et al., 2016) and **voltage-dependent Ca^{2+} channels** (Atlas, 2014). For example, in the hippocampus, regulation of the release of the neurotransmitter **gamma-aminobutyric acid (GABA)** by ionotropic glutamate kainate receptors involves activation of PLC and protein kinase C via a Pertussis toxin–sensitive G protein rather ion flux through the channel (Rodríguez-Moreno & Lerma, 1998). While the kainate receptor is normally considered to be an ion channel, the results reveal an additional metabotropic coupling of the channel to a second messenger signalling cascade (Rodríguez-Moreno & Lerma, 1998).

Further support for the proposal that IP_3R may be involved in roles that are separate from the channel's Ca^{2+} release function is found in the relatively small number of the overall complement of IP_3R that appear to be involved in Ca^{2+} release. There is a dense distribution of IP_3Rs through the cell, as can be seen in Figure S3Ai, and radioligand assays report there are about 30,000 IP_3R monomers (IP_3 binding sites) per cell (Smith et al., 2014; Taylor & Konieczny, 2016; Wilson et al., 1998). However, Ca^{2+} release occurs from only a few hundred of these IP_3Rs and active channels are restricted to small clusters at discrete sites. IP_3-evoked Ca^{2+} release, therefore, occurs in only about 3% of the overall IP_3R complement of the cell (Smith et al., 2009; Smith & Parker, 2009). The great majority of IP_3Rs bind IP_3 but appear to be functionally 'silent', at least in terms of IP_3-mediated Ca^{2+} release (Parker & Smith, 2010; Taylor & Konieczny, 2016). It is tempting to speculate that some of these 'silent' IP_3R may contribute to additional functions of IP_3, such as acting to mediate PLC-dependent IP_3-induced IP_3 production. Unravelling the precise mechanisms by which IP_3 induces additional IP_3 production presents a considerable challenge. Systematic and high-throughput screens may be required to unravel the mechanisms. RNA interference screens have successfully demonstrated previously unknown components of biological pathways, such as stromal interaction molecule (STIM) (Liou et al., 2005; Roos et al., 2005) and may be useful in identifying components of the IP_3 signalling pathway. However, it is noteworthy that the links between Ca^{2+} store depletion and store-operated Ca^{2+} entry was a prolonged effort that required many years of work, a large number of laboratories and numerous false leads. The eventual discovery of STIM and its interaction with Orai marked the culmination of these extensive endeavours.

Gap junctions are a major route of cell–cell communication (Pohl, 2020). Gap junctions form the link for electrical coupling by allowing intercellular diffusion of current-carrying ions and provide the route for several types of metabolites and second messenger molecules to diffuse among cells. However, our results suggest that gap junctions, acting as pores for the diffusion of intercellular messengers, do not contribute to wave propagation. First, we show that diffusion speeds via gap junctions are too slow to contribute significantly to wave propagation. cIP_3-induced Ca^{2+} waves occurs at 73 $\mu m \cdot s^{-1}$ rate of change of fluorescence over distance, while the rate of change over distance for the small molecular weight fluorophore calcein (close in size to IP_3) is 0.01 $\mu m \cdot s^{-1}$. Based on their molecular masses, the rate

of change of calcein should be ~1.2 times slower than that of IP_3. The measured rate of change of fluorescence intensity for calcein was >5000-fold slower than the Ca^{2+} waves. The slow rate for calcein presumably reflects a very low permeability between cells.

Second, Ca^{2+} did not diffuse into neighbouring cells after photolysis of caged Ca^{2+} or endothelial activation with ionomycin - even when the endothelium was pre-activated by ACh. If gap junctions were open, an increased Ca^{2+} would be expected to diffuse passively into neighbouring cells; this was not observed.

Third, blocking gap junctions did not inhibit wave propagation. The gap junction inhibitor 18α-glycyrrhetinic acid effectively stopped the diffusion of fluorophores between cells, consistent with its reported inhibitory effect at gap junctions. However, the inhibitor did not block the propagation of Ca^{2+} waves. These findings question the involvement of gap junctions as a pore for the diffusion of second messengers in Ca^{2+} wave propagation in intact (uninjured) endothelium.

Our results also suggest that Ca^{2+} itself does not contribute to wave propagation. Two observations support this conclusion. First, release of caged Ca^{2+} or Ca^{2+} rises by locally applied ionomycin do not evoke a Ca^{2+} wave. The amplitude of the Ca^{2+} rise evoked by ionomycin and release of Ca^{2+} via photolysis of cNP-EGTA was similar to that generated by ACh and caged IP_3; therefore, the lack of intercellular communication cannot be explained by failure to reach a threshold level of Ca^{2+}. Second, when Ca^{2+} was locally buffered, IP_3 still evoked a Ca^{2+} wave.

The mechanisms underlying intercellular Ca^{2+} waves appear to depend on cell type. In some, most notably in cultured cell lines, elevation of extracellular ATP triggers an IP_3-dependent Ca^{2+} increase (Ceriani et al., 2016; Osipchuk & Cahalan, 1992). The elevated Ca^{2+} increases connexin or pannexin channel open probability resulting in the release of ATP from cells. Released ATP binds to P_2Y receptors (Gale et al., 2004; Piazza et al., 2007) of nearby cells (Rodriguez et al., 2012) and activates PLC-dependent IP_3 production. This in turn promotes Ca^{2+} release from intracellular stores increasing hemichannel open probability (De Vuyst et al., 2006, 2009; Leybaert et al., 2003), promoting further ATP release in a self-regenerative cascade that propagates Ca^{2+} waves across the cell network. This process does not appear to contribute to wave propagation in the endothelium when there is structural proximity of cells. If a diffusible extracellular messenger were a significant contributor to wave propagation, rapid extracellular fluid flow would have been expected to bias the direction of wave propagation. However, various directions of extracellular fluid flow did not alter the direction or extent of wave propagation. Furthermore, the hydrolysis of extracellular ATP with apyrase or ATP receptor blockers did not alter wave propagation in either the intact preparation or in endothelial patches, either in male or female rats. These results suggest that ATP as a diffusible messenger is unlikely to be involved in wave transmission in the absence of an endothelial discontinuity.

Intercellular Ca^{2+} waves that involve a diffusible extracellular messenger are able to cross distances in which there are no direct connections between cells (Cotrina et al., 1998; Gomes, Srinivas, Vereecke, & Himpens, 2005; Guthrie et al., 1999; Hassinger et al., 1996). Our results show that when there is structural proximity of adjacent cells a diffusible messenger is not involved in intercellular wave propagation. However, Ca^{2+} wave propagation does not halt where there is discontinuity in cell contact. When the structural proximity of adjacent cells is disrupted, the mechanism underlying wave propagation switches from IP_3-induced IP_3 release to a diffusible messenger that maintains signalling across the discontinuity. There was, however, a small but significant reduction in magnitude of propagated vasodilation beyond the discontinuity.

Support for the involvement of a diffusible messenger in wave transmission, when there was a discontinuity, was found in the observations that wave propagation was altered by extracellular fluid flow and blocked by hydrolysis of ATP or by ATP receptor inhibitors. These findings suggest that the diffusible messenger is ATP.

Our results highlight two mechanisms in maintaining Ca^{2+} wave propagation in the endothelium in intact blood vessels (Figure 8). In other systems, two mechanisms may also contribute to Ca^{2+} wave spread between cell populations (Braet et al., 2001; Charles, 1998; Grafstein et al., 2000; Paemeleire et al., 2000; Scemes et al., 2000). In spinal cord astrocytes cultured from neonatal mice, Cx43 is required for wave propagation to occur. However, in Cx43 knockout mice, intercellular waves propagated with the same velocity and amplitude and to the same number of cells as astrocytes cultured from wild-type mice. Astrocytes from Cx43 knockout neonatal mice had a compensatory increase in autocrine communication to maintain wave propagation (Scemes et al., 2000).

In our study, direct cell contact appears to disable the ATP wave transmission pathway. When there is direct cell contact, wave propagation was unaltered by extracellular fluid flow, ATP hydrolysis or ATP receptor block. These results indicate a diffusible messenger is an unlikely contributor to wave propagation when there is direct cell contact. The mechanism that underlies the signalling switch enabling ATP release when cell contact is disrupted is unclear. However, our study shows that after contact between cells was disrupted, Cx43 was exposed at the surface of the discontinuity. 'Disengaged' Cx43 hemichannels may provide the route for ATP release (Kang et al., 2008). Whatever the mechanism, the intercellular signalling switch bestows robustness and sensitivity to intercellular communication.

Ca^{2+} waves are significant in cell–cell communication and occur in various cell types and tissues (Charles et al., 1992; Kasai, 1995; Leybaert & Sanderson, 2012; Robb-Gaspers & Thomas, 1995). In the endothelium, local activation may evoke propagating Ca^{2+} waves that bring about an increased blood flow as a result of 'ascending vasodilation' (Domeier & Segal, 2007; Longden et al., 2017, 2021; Tallini et al., 2007; Uhrenholt et al., 2007). While the mesenteric is an excellent model of resistance artery function, the precise molecular, cellular and integrative mechanisms for blood flow control in organ systems such as the brain and other areas such as skeletal muscle may show differing specializations. It will be important to understand conserved and nonconserved mechanisms of endothelial communication and resulting blood pressure control in these vascular beds, particularly because our recent studies show that communication is critical for conveying information from the orchestrated chemical and

mechanical cues that drive endothelial function and for emergent behaviour to occur (Lee et al., 2018, 2022; McCarron et al., 2017, 2019; Wilson et al., 2020; Wilson, Saunter, et al., 2016b; Zhang et al., 2019).

Previous mathematical models have suggested the existence of IP_3-induced IP_3 production as a mechanism to account for intercellular Ca^{2+} waves, but experimental evidence has been lacking (Cuthbertson & Chay, 1991; Sneyd et al., 1994). Our results suggest that IP_3 either directly or indirectly activates phospholipase C in neighbouring cells. In the face of self-reinforcing IP_3-induced IP_3 production, the question arises as to how IP_3 production and Ca^{2+} release are terminated. Even if IP_3 is generated only in neighbouring cells, there may be back propagation of signals. Local depletion of PIP2, negative feedback effects of protein kinase C on PLC (Ryu et al., 1990; Xu et al., 2001), or effects of Ca^{2+} on IP_3 generation may provide intrinsic mechanisms to terminate IP_3 production.

Communication among cells in the endothelium is critical for transmitting the information that propagates the vasodilation underlying the local regulation of blood flow as tissue metabolic requirements change. Our results reveal a novel mechanism, IP_3-induced IP_3 production that provides the principal route by which endothelial cells transmit information that enables propagated vasodilation (Figure 8). We also show that, when the endothelium is damaged, communication and propagated vasodilation is maintained by the release and diffusion of ATP across an endothelial discontinuity (Figure 8). Our results show that a switch between regenerative IP_3-mediated IP_3 release in intact arteries and ATP-driven propagation across endothelial discontinuities maintains the communication required for cardiovascular function to occur.

AUTHOR CONTRIBUTIONS

C. Buckley: Conceptualization (equal); data curation (equal); formal analysis (equal); funding acquisition (equal); investigation (equal); methodology (equal); project administration (equal); software (equal); supervision (equal); writing—original draft (equal); writing—review and editing (equal). **M. D. Lee:** Software (equal); writing—original draft (equal); writing—review and editing (equal). **X. Zhang:** Software (equal); writing—original draft (equal); writing—review and editing (equal). **C. Wilson:** Funding acquisition (equal); project administration (equal); software; writing—original draft (equal); writing—review and editing (equal). J. G. McCarron: Conceptualization (equal); data curation (equal); formal analysis (equal); funding acquisition (equal); investigation (equal); methodology (equal); project administration (equal); software (equal); supervision (equal); writing—original draft (equal); writing—review and editing (equal).

ACKNOWLEDGEMENTS

This work was funded by the British Heart Foundation (RG/F/20/110007 and PG/20/9/34859) whose support is gratefully acknowledged. The authors would like to thank Margaret MacDonald for her excellent technical support. The authors gratefully acknowledge Aberdeen Microscopy and Histology Core Facility, in particular Debbie Wilkinson, for their support & assistance in this work and Prof Alexi Tepikin (University of Liverpool) who kindly provided Diazo-2/AM.

CONFLICT OF INTEREST STATEMENT

There are no competing interests.

DATA AVAILABILITY STATEMENT

All study data are included in the article and supporting information.

DECLARATION OF TRANSPARENCY AND SCIENTIFIC RIGOUR

This declaration acknowledges that this paper adheres to the principles for transparent reporting and scientific rigour of preclinical research as stated in the BJP guidelines for Design and Analysis, Immunoblotting and Immunochemistry and Animal Experimentation and as recommended by funding agencies, publishers and other organizations engaged with supporting research.

ORCID

Matthew D. Lee https://orcid.org/0000-0001-8265-382X
Calum Wilson https://orcid.org/0000-0003-2500-0632
John G. McCarron https://orcid.org/0000-0002-3302-3984

REFERENCES

Alexander, S. P. H., Kelly, E., Mathie, A. A., Peters, J. A., Veale, E. L., Armstrong, J. F., Buneman, O. P., Faccenda, E., Harding, S. D., Spedding, M., Cidlowski, J. A., Fabbro, D., Davenport, A. P., Striessnig, J., Davies, J. A., Ahlers-Dannen, K. E., Alqinyah, M., Arumugam, T. V., Bodle, C., … Zolghadri, Y. (2023). The Concise Guide to PHARMACOLOGY 2023/24: Introduction and Other Protein Targets. *British Journal of Pharmacology*, *180*, S1–S22. https://doi.org/10.1111/bph.16176

Alexander, S. P. H., Christopoulos, A., Davenport, A. P., Kelly, E., Mathie, A. A., Peters, J. A., Veale, E. L., Armstrong, J. F., Faccenda, E., Harding, S. D., Davies, J. A., Abbracchio, M. P., Abraham, G., Agoulnik, A., Alexander, W., Al-Hosaini, K., Bäck, M., Baker, J. G., … Ye, R. D. (2023). The Concise Guide to PHARMACOLOGY 2023/24: G protein-coupled receptors. *British Journal of Pharmacology*, *180*, S23–S144. https://doi.org/10.1111/bph.16177

Alexander, S. P. H., Mathie, A. A., Peters, J. A., Veale, E. L., Striessnig, J., Kelly, E., Armstrong, J. F., Faccenda, E., Harding, S. D., Davies, J. A., Aldrich, R. W., Attali, B., Baggetta, A. M., Becirovic, E., Biel, M., Bill, R. M., Caceres, A. I., Catterall, W. A., Conner, A. C., … Zhu, M. (2023). The Concise Guide to PHARMACOLOGY 2023/24: Ion channels. *British Journal of Pharmacology*, *180*, S145–S222. https://doi.org/10.1111/bph.16178

Alexander, S. P. H., Fabbro, D., Kelly, E., Mathie, A. A., Peters, J. A., Veale, E. L., Armstrong, J. F., Faccenda, E., Harding, S. D., Davies, J. A., Annett, S., Boison, D., Burns, K. E., Dessauer, C., Gertsch, J., Helsby, N. A., Izzo, A. A., Ostrom, R., Papapetropoulos, A., … Wong, S. S. (2023). The Concise Guide to PHARMACOLOGY 2023/24: Enzymes. *British Journal of Pharmacology*, *180*, S289–S373. https://doi.org/10.1111/bph.16181

Alexander, S. P. H., Roberts, R. E., Broughton, B. R. S., Sobey, C. G., George, C. H., Stanford, S. C., Cirino, G., Docherty, J. R., Giembycz, M. A., Hoyer, D., Insel, P. A., Izzo, A. A., Ji, Y., MacEwan, D. J., Mangum, J., Wonnacott, S., & Ahluwalia, A. (2018). Goals and practicalities of immunoblotting and immunohistochemistry: A guide for submission to the *British Journal of Pharmacology*. *British Journal of Pharmacology*, *175*, 407–411. https://doi.org/10.1111/bph.14112

Allbritton, N. L., Meyer, T., & Stryer, L. (1992). Range of messenger action of calcium ion and inositol 1,4,5-trisphosphate. *Science*, *258*, 1812–1815. https://doi.org/10.1126/science.1465619

Atlas, D. (2014). Voltage-gated calcium channels function as Ca^{2+}-activated signaling receptors. *Trends in Biochemical Sciences*, *39*, 45–52. https://doi.org/10.1016/j.tibs.2013.12.005

Balla, A., Tuymetova, G., Toth, B., Szentpetery, Z., Zhao, X., Knight, Z. A., Shokat, K., Steinbach, P. J., & Balla, T. (2008). Design of drug-resistant alleles of type-III phosphatidylinositol 4-kinases using mutagenesis and molecular modeling. *Biochemistry*, *47*, 1599–1607. https://doi.org/10.1021/bi7017927

Bao, L., Locovei, S., & Dahl, G. (2004). Pannexin membrane channels are mechanosensitive conduits for ATP. *FEBS Letters*, *572*, 65–68. https://doi.org/10.1016/j.febslet.2004.07.009

Bartok, A., Weaver, D., Golenár, T., Nichtova, Z., Katona, M., Bánsághi, S., Alzayady, K. J., Thomas, V. K., Ando, H., Mikoshiba, K., Joseph, S. K., Yule, D. I., Csordás, G., & Hajnóczky, G. (2019). IP3 receptor isoforms differently regulate ER-mitochondrial contacts and local calcium transfer. *Nature Communications*, *10*, 3726. https://doi.org/10.1038/s41467-019-11646-3

Bennett, M. V., Barrio, L. C., Bargiello, T. A., Spray, D. C., Hertzberg, E., & Sáez, J. C. (1991). Gap junctions: New tools, new answers, new questions. *Neuron*, *6*, 305–320. https://doi.org/10.1016/0896-6273(91)90241-Q

Boitano, S., Dirksen, E. R., & Sanderson, M. J. (1992). Intercellular propagation of calcium waves mediated by inositol trisphosphate. *Science*, *258*, 292–295. https://doi.org/10.1126/science.1411526

Braet, K., Paemeleire, K., D'Herde, K., Sanderson, M. J., & Leybaert, L. (2001). Astrocyte-endothelial cell calcium signals conveyed by two signalling pathways. *The European Journal of Neuroscience*, *13*, 79–91.

Breer, H., Boekhoff, I., & Tareilus, E. (1990). Rapid kinetics of second messenger formation in olfactory transduction. *Nature*, *345*, 65–68. https://doi.org/10.1038/345065a0

Buckley, C., Wilson, C., & McCarron, J. G. (2020). FK506 regulates Ca^{2+} release evoked by inositol 1,4,5-trisphosphate independently of FK-binding protein in endothelial cells. *British Journal of Pharmacology*, *177*, 1131–1149. https://doi.org/10.1111/bph.14905

Buckley, C., Zhang, X., Wilson, C., & McCarron, J. G. (2021). Carbenoxolone and 18β-glycyrrhetinic acid inhibit inositol 1,4,5-trisphosphate-mediated endothelial cell calcium signalling and depolarise mitochondria. *British Journal of Pharmacology*, *178*, 896–912. https://doi.org/10.1111/bph.15329

Burgess, G. M., McKinney, J. S., Irvine, R. F., & Putney, J. W. Jr. (1985). Inositol 1,4,5-trisphosphate and inositol 1,3,4-trisphosphate formation in Ca^{2+}-mobilizing-hormone-activated cells. *The Biochemical Journal*, *232*, 237–243. https://doi.org/10.1042/bj2320237

Ceriani, F., Pozzan, T., & Mammano, F. (2016). Critical role of ATP-induced ATP release for Ca^{2+} signaling in nonsensory cell networks of the developing cochlea. *Proceedings of the National Academy of Sciences of the United States of America*, *113*, E7194–E7201.

Chakraborty, P., Deb, B. K., Taylor, C. W., & Hasan, G. (2022). Regulation of store-operated Ca^{2+} entry by IP3 receptors independent of their ability to release Ca^{2+}. *Elife*, *12*, 488111.

Charles, A. (1998). Intercellular calcium waves in glia. *Glia*, *24*, 39–49. https://doi.org/10.1002/(SICI)1098-1136(199809)24:1<39::AID-GLIA5>3.0.CO;2-W

Charles, A. C., Naus, C. C., Zhu, D., Kidder, G. M., Dirksen, E. R., & Sanderson, M. J. (1992). Intercellular calcium signaling via gap junctions in glioma cells. *The Journal of Cell Biology*, *118*, 195–201. https://doi.org/10.1083/jcb.118.1.195

Chepkova, A. N., Sergeeva, O. A., & Haas, H. L. (2008). Carbenoxolone impairs LTP and blocks NMDA receptors in murine hippocampus. *Neuropharmacology*, *55*, 139–147. https://doi.org/10.1016/j.neuropharm.2008.05.001

Cotrina, M. L., Lin, J. H., Alves-Rodrigues, A., Liu, S., Li, J., Azmi-Ghadimi, H., Kang, J., Naus, C. C., & Nedergaard, M. (1998). Connexins regulate calcium signaling by controlling ATP release. *Proceedings of the National Academy of Sciences of the United States of America*, *95*, 15735–15740. https://doi.org/10.1073/pnas.95.26.15735

Curtis, M. J., Alexander, S., Cirino, G., Docherty, J. R., George, C. H., Giembycz, M. A., Hoyer, D., Insel, P. A., Izzo, A. A., Ji, Y., MacEwan, D. J., Sobey, C. G., Stanford, S. C., Teixeira, M. M., Wonnacott, S., & Ahluwalia, A. (2018). Experimental design and analysis and their reporting II: Updated and simplified guidance for authors and peer reviewers. *British Journal of Pharmacology*, *175*, 987–993. https://doi.org/10.1111/bph.14153

Cuthbertson, K. S., & Chay, T. R. (1991). Modelling receptor-controlled intracellular calcium oscillators. *Cell Calcium*, *12*, 97–109. https://doi.org/10.1016/0143-4160(91)90012-4

Dai, J., Patzke, C., Liakath-Ali, K., Seigneur, E., & Südhof, T. C. (2021). GluD1 is a signal transduction device disguised as an ionotropic receptor. *Nature*, *595*, 261–265. https://doi.org/10.1038/s41586-021-03661-6

De Vuyst, E., Decrock, E., Cabooter, L., Dubyak, G. R., Naus, C. C., Evans, W. H., & Leybaert, L. (2006). Intracellular calcium changes trigger connexin 32 hemichannel opening. *The EMBO Journal*, *25*, 34–44. https://doi.org/10.1038/sj.emboj.7600908

De Vuyst, E., Wang, N., Decrock, E., De Bock, M., Vinken, M., Van Moorhem, M., Lai, C., Culot, M., Rogiers, V., Cecchelli, R., Naus, C. C., Evans, W. H., & Leybaert, L. (2009). Ca^{2+} regulation of connexin 43 hemichannels in C6 glioma and glial cells. *Cell Calcium*, *46*, 176–187. https://doi.org/10.1016/j.ceca.2009.07.002

de Wit, C., Roos, F., Bolz, S. S., Kirchhoff, S., Krüger, O., Willecke, K., & Pohl, U. (2000). Impaired conduction of vasodilation along arterioles in connexin40-deficient mice. *Circulation Research*, *86*, 649–655. https://doi.org/10.1161/01.RES.86.6.649

de Wit, C., Roos, F., Bolz, S.-S., & Pohl, U. (2003). Lack of vascular connexin 40 is associated with hypertension and irregular arteriolar vasomotion. *Physiological Genomics*, *13*, 169–177.

Dickinson, G. D., Ellefsen, K. L., Dawson, S. P., Pearson, J. E., & Parker, I. (2016). Hindered cytoplasmic diffusion of inositol trisphosphate restricts its cellular range of action. *Science Signaling*, *9*, ra108. https://doi.org/10.1126/scisignal.aag1625

Domeier, T. L., & Segal, S. S. (2007). Electromechanical and pharmacomechanical signalling pathways for conducted vasodilatation along endothelium of hamster feed arteries. *The Journal of Physiology*, *579*, 175–186. https://doi.org/10.1113/jphysiol.2006.124529

Figueroa, X. F., & Duling, B. R. (2008). Dissection of two Cx37-independent conducted vasodilator mechanisms by deletion of Cx40: Electrotonic versus regenerative conduction. *American Journal of Physiology. Heart and Circulatory Physiology*, *295*, H2001–H2007. https://doi.org/10.1152/ajpheart.00063.2008

Figueroa, X. F., Isakson, B. E., & Duling, B. R. (2004). Connexins: Gaps in our knowledge of vascular function. *Physiology Bethesda Md*, *19*, 277–284. https://doi.org/10.1152/physiol.00008.2004

Filiberto, A. C., Spinosa, M. D., Elder, C. T., Su, G., Leroy, V., Ladd, Z., Lu, G., Mehaffey, J. H., Salmon, M. D., Hawkins, R. B., Ravichandran, K. S., Isakson, B. E., Upchurch, G. R. Jr., & Sharma, A. K. (2022). Endothelial pannexin-1 channels modulate macrophage and smooth muscle cell activation in abdominal aortic aneurysm formation. *Nature Communications*, *13*, 1521. https://doi.org/10.1038/s41467-022-29233-4

Gale, J. E., Piazza, V., Ciubotaru, C. D., & Mammano, F. (2004). A mechanism for sensing noise damage in the inner ear. *Current Biology CB*, *14*, 526–529. https://doi.org/10.1016/j.cub.2004.03.002

Gomes, P., Srinivas, S. P., Van Driessche, W., Vereecke, J., & Himpens, B. (2005). ATP release through connexin hemichannels in corneal endothelial cells. *Investigative Ophthalmology & Visual Science*, *46*, 1208–1218. https://doi.org/10.1167/iovs.04-1181

Gomes, P., Srinivas, S. P., Vereecke, J., & Himpens, B. (2005). ATP-dependent paracrine intercellular communication in cultured bovine corneal endothelial cells. *Investigative Ophthalmology & Visual Science*, *46*, 104–113. https://doi.org/10.1167/iovs.04-0846

Grafstein, B., Liu, S., Cotrina, M. L., Goldman, S. A., & Nedergaard, M. (2000). Meningeal cells can communicate with astrocytes by calcium signaling. *Annals of Neurology*, *47*, 18–25. https://doi.org/10.1002/1531-8249(200001)47:1<18::AID-ANA6>3.0.CO;2-N

Guthrie, P. B., Knappenberger, J., Segal, M., Bennett, M. V. L., Charles, A. C., & Kater, S. B. (1999). ATP released from astrocytes mediates glial calcium waves. *The Journal of Neuroscience*, *19*, 520–528. https://doi.org/10.1523/JNEUROSCI.19-02-00520.1999

Harraz, O. F., Longden, T. A., Hill-Eubanks, D., & Nelson, M. T. (2018). PIP2 depletion promotes TRPV4 channel activity in mouse brain capillary endothelial cells. *eLife*, *7*, e38689. https://doi.org/10.7554/eLife.38689

Hassinger, T. D., Guthrie, P. B., Atkinson, P. B., Bennett, M. V. L., & Kater, S. B. (1996). An extracellular signaling component in propagation of astrocytic calcium waves. *Proceedings of the National Academy of Sciences*, *93*, 13268–13273. https://doi.org/10.1073/pnas.93.23.13268

Isakson, B. E., Ramos, S. I., & Duling, B. R. (2007). Ca^{2+} and inositol 1,4,5-trisphosphate-mediated signaling across the myoendothelial junction. *Circulation Research*, *100*, 246–254. https://doi.org/10.1161/01.RES.0000257744.23795.93

Jiménez-Pérez, L., Cidad, P., Álvarez-Miguel, I., Santos-Hipólito, A., Torres-Merino, R., Alonso, E., de la Fuente, M. Á., López-López, J. R., & Pérez-García, M. T. (2016). Molecular determinants of Kv1.3 potassium channels-induced proliferation*. *The Journal of Biological Chemistry*, *291*, 3569–3580. https://doi.org/10.1074/jbc.M115.678995

Kang, J., Kang, N., Lovatt, D., Torres, A., Zhao, Z., Lin, J., & Nedergaard, M. (2008). Connexin 43 hemichannels are permeable to ATP. *Journal of Neuroscience: The Official Journal of the Society for Neuroscience*, *28*, 4702–4711. https://doi.org/10.1523/JNEUROSCI.5048-07.2008

Kasai, H. (1995). Pancreatic calcium waves and secretion. *Ciba Foundation Symposium*, *188*, 104–116; discussion 116-120. https://doi.org/10.1002/9780470514696.ch7

Khan, M. T., Bhanumathy, C. D., Schug, Z. T., & Joseph, S. K. (2007). Role of inositol 1,4,5-trisphosphate receptors in apoptosis in DT40 lymphocytes. *The Journal of Biological Chemistry*, *282*, 32983–32990. https://doi.org/10.1074/jbc.M705183200

Krüger, O., Bény, J.-L., Chabaud, F., Traub, O., Theis, M., Brix, K., Kirchhoff, S., & Willecke, K. (2002). Altered dye diffusion and upregulation of connexin37 in mouse aortic endothelium deficient in connexin40. *Journal of Vascular Research*, *39*, 160–172. https://doi.org/10.1159/000057764

Kurjiaka, D. T. (2004). The conduction of dilation along an arteriole is diminished in the cremaster muscle of hypertensive hamsters. *Journal of Vascular Research*, *41*, 517–524. https://doi.org/10.1159/000081808

Kurth-Nelson, Z. L., Mishra, A., & Newman, E. A. (2009). Spontaneous glial calcium waves in the retina develop over early adulthood. *Journal of Neuroscience: The Official Journal of the Society for Neuroscience*, *29*, 11339–11346. https://doi.org/10.1523/JNEUROSCI.2493-09.2009

Lawton, P. F., Lee, M. D., Saunter, C. D., Girkin, J. M., McCarron, J. G., & Wilson, C. (2019). VasoTracker, a low-cost and open source pressure myograph system for vascular physiology. *Frontiers in Physiology*, *10*, 99. https://doi.org/10.3389/fphys.2019.00099

Lee, M. D., Buckley, C., Zhang, X., Louhivuori, L., Uhlén, P., Wilson, C., & McCarron, J. G. (2022). Small-world connectivity dictates collective endothelial cell signaling. *Proceedings of the National Academy of Sciences*, *119*, e2118927119. https://doi.org/10.1073/pnas.2118927119

Lee, M. D., Wilson, C., Saunter, C. D., Kennedy, C., Girkin, J. M., & McCarron, J. G. (2018). Spatially structured cell populations process multiple sensory signals in parallel in intact vascular endothelium. *Science Signaling*, *11*, eaar4411. https://doi.org/10.1126/scisignal.aar4411

Leybaert, L., Braet, K., Vandamme, W., Cabooter, L., Martin, P. E. M., & Evans, W. H. (2003). Connexin channels, connexin mimetic peptides and ATP release. *Cell Communication & Adhesion*, *10*, 251–257. https://doi.org/10.1080/cac.10.4-6.251.257

Leybaert, L., Paemeleire, K., Strahonja, A., & Sanderson, M. J. (1998). Inositol-trisphosphate-dependent intercellular calcium signaling in and between astrocytes and endothelial cells. *Glia*, *24*, 398–407. https://doi.org/10.1002/(SICI)1098-1136(199812)24:4<398::AID-GLIA5>3.0.CO;2-R

Leybaert, L., & Sanderson, M. J. (2012). Intercellular Ca^{2+} waves: Mechanisms and function. *Physiological Reviews*, *92*, 1359–1392. https://doi.org/10.1152/physrev.00029.2011

Lilley, E., Stanford, S. C., Kendall, D. E., Alexander, S. P. H., Cirino, G., Docherty, J. R., George, C. H., Insel, P. A., Izzo, A. A., Ji, Y., Panettieri, R. A., Sobey, C. G., Stefanska, B., Stephens, G., Teixeira, M., & Ahluwalia, A. (2020). ARRIVE 2.0 and the British Journal of Pharmacology: Updated guidance for 2020. *British Journal of Pharmacology*, *177*, 3611–3616. https://doi.org/10.1111/bph.15178

Liou, J., Kim, M. L., Do Heo, W., Jones, J. T., Myers, J. W., Ferrell, J. E., & Meyer, T. (2005). STIM is a Ca^{2+} sensor essential for Ca^{2+}-store-depletion-triggered Ca^{2+} influx. *Current Biology*, *15*, 1235–1241. https://doi.org/10.1016/j.cub.2005.05.055

Longden, T. A., Dabertrand, F., Koide, M., Gonzales, A. L., Tykocki, N. R., Brayden, J. E., Hill-Eubanks, D., & Nelson, M. T. (2017). Capillary K+-sensing initiates retrograde hyperpolarization to increase local cerebral blood flow. *Nature Neuroscience*, *20*, 717–726. https://doi.org/10.1038/nn.4533

Longden, T. A., Mughal, A., Hennig, G. W., Harraz, O. F., Shui, B., Lee, F. K., Lee, J. C., Reining, S., Kotlikoff, M. I., König, G. M., Kostenis, E., Hill-Eubanks, D., & Nelson, M. T. (2021). Local IP3 receptor–mediated Ca^{2+} signals compound to direct blood flow in brain capillaries. *Science Advances*, *7*, eabh0101. https://doi.org/10.1126/sciadv.abh0101

MacMillan, D., & McCarron, J. (2010). The phospholipase C inhibitor U-73122 inhibits Ca^{2+} release from the intracellular sarcoplasmic reticulum Ca^{2+} store by inhibiting Ca^{2+} pumps in smooth muscle. *British Journal of Pharmacology*, *160*, 1295–1301. https://doi.org/10.1111/j.1476-5381.2010.00771.x

Mahaut-Smith, M. P., Hussain, J. F., & Mason, M. J. (1999). Depolarization-evoked Ca^{2+} release in a non-excitable cell, the rat megakaryocyte. *The Journal of Physiology*, *515*, 385–390. https://doi.org/10.1111/j.1469-7793.1999.385ac.x

McCarron, J. G., Chalmers, S., MacMillan, D., & Olson, M. L. (2010). Agonist-evoked Ca^{2+} wave progression requires Ca^{2+} and IP_3. *Journal of Cellular Physiology*, *224*, 334–344. https://doi.org/10.1002/jcp.22103

McCarron, J. G., Flynn, E. R. M., Bradley, K. N., & Muir, T. C. (2000). Two Ca^{2+} entry pathways mediate InsP3-sensitive store refilling in guinea-pig colonic smooth muscle. *The Journal of Physiology*, *525*, 113–124. https://doi.org/10.1111/j.1469-7793.2000.00113.x

McCarron, J. G., Lee, M. D., & Wilson, C. (2017). The endothelium solves problems that endothelial cells do not know exist. *Trends in Pharmacological Sciences*, *38*, 322–338. https://doi.org/10.1016/j.tips.2017.01.008

McCarron, J. G., Wilson, C., Heathcote, H. R., Zhang, X., Buckley, C., & Lee, M. D. (2019). Heterogeneity and emergent behaviour in the vascular endothelium. *Current Opinion in Pharmacology*, *45*, 23–32. https://doi.org/10.1016/j.coph.2019.03.008

Osipchuk, Y., & Cahalan, M. (1992). Cell-to-cell spread of calcium signals mediated by ATP receptors in mast cells. *Nature*, *359*, 241–244. https://doi.org/10.1038/359241a0

Paemeleire, K., Martin, P. E. M., Coleman, S. L., Fogarty, K. E., Carrington, W. A., Leybaert, L., Tuft, R. A., Evans, W. H., &

Sanderson, M. J. (2000). Intercellular calcium waves in HeLa cells expressing GFP-labeled connexin 43, 32, or 26. *Molecular Biology of the Cell*, *11*, 1815–1827. https://doi.org/10.1091/mbc.11.5.1815

Parker, I., & Smith, I. F. (2010). Recording single-channel activity of inositol trisphosphate receptors in intact cells with a microscope, not a patch clamp. *The Journal of General Physiology*, *136*, 119–127. https://doi.org/10.1085/jgp.200910390

Percie Du Sert, N., Hurst, V., Ahluwalia, A., Alam, S., Avey, M. T., Baker, M., Browne, W. J., Clark, A., Cuthill, I. C., Dirnagl, U., Emerson, M., Garner, P., Holgate, S. T., Howells, D. W., Karp, N. A., Lazic, S. E., Lidster, K., MacCallum, C. J., & Macleod, M. (2020). The ARRIVE guidelines 2.0: Updated guidelines for reporting animal research. *PLoS Biology*, *18*, e3000410. https://doi.org/10.1371/journal.pbio.3000410

Piazza, V., Ciubotaru, C. D., Gale, J. E., & Mammano, F. (2007). Purinergic signalling and intercellular Ca^{2+} wave propagation in the organ of Corti. *Cell Calcium*, *41*, 77–86. https://doi.org/10.1016/j.ceca.2006.05.005

Pohl, U. (2020). Connexins: Key players in the control of vascular plasticity and function. *Physiological Reviews*, *100*, 525–572. https://doi.org/10.1152/physrev.00010.2019

Robb-Gaspers, L. D., & Thomas, A. P. (1995). Coordination of Ca^{2+} signaling by intercellular propagation of Ca^{2+} waves in the intact liver (*). *The Journal of Biological Chemistry*, *270*, 8102–8107. https://doi.org/10.1074/jbc.270.14.8102

Rodriguez, L., Simeonato, E., Scimemi, P., Anselmi, F., Calì, B., Crispino, G., Ciubotaru, C. D., Bortolozzi, M., Ramirez, F. G., Majumder, P., Arslan, E., de Camilli, P., Pozzan, T., & Mammano, F. (2012). Reduced phosphatidylinositol 4,5-bisphosphate synthesis impairs inner ear Ca^{2+} signaling and high-frequency hearing acquisition. *Proceedings of the National Academy of Sciences*, *109*, 14013–14018. https://doi.org/10.1073/pnas.1211869109

Rodríguez-Moreno, A., & Lerma, J. (1998). Kainate receptor modulation of GABA release involves a metabotropic function. *Neuron*, *20*, 1211–1218. https://doi.org/10.1016/S0896-6273(00)80501-2

Roos, J., DiGregorio, P. J., Yeromin, A. V., Ohlsen, K., Lioudyno, M., Zhang, S., Safrina, O., Kozak, J. A., Wagner, S. L., Cahalan, M. D., Veliçelebi, G., & Stauderman, K. A. (2005). STIM1, an essential and conserved component of store-operated Ca^{2+} channel function. *The Journal of Cell Biology*, *169*, 435–445. https://doi.org/10.1083/jcb.200502019

Ryu, S. H., Kim, U. H., Wahl, M. I., Brown, A. B., Carpenter, G., Huang, K. P., & Rhee, S. G. (1990). Feedback regulation of phospholipase C-beta by protein kinase C. *The Journal of Biological Chemistry*, *265*, 17941–17945. https://doi.org/10.1016/S0021-9258(18)38254-1

Saez, J. C., Berthoud, V. M., Branes, M. C., Martinez, A. D., & Beyer, E. C. (2003). Plasma membrane channels formed by connexins: Their regulation and functions. *Physiological Reviews*, *83*, 1359–1400. https://doi.org/10.1152/physrev.00007.2003

Salvi, M., Fiore, C., Battaglia, V., Palermo, M., Armanini, D., & Toninello, A. (2005). Carbenoxolone induces oxidative stress in liver mitochondria, which is responsible for transition pore opening. *Endocrinology*, *146*, 2306–2312. https://doi.org/10.1210/en.2004-1128

Sanderson, M. J. (1995). Intercellular calcium waves mediated by inositol trisphosphate. *Ciba Foundation Symposium*, *188*, 175–189. discussion 189-194

Scemes, E., Suadicani, S. O., & Spray, D. C. (2000). Intercellular communication in spinal cord astrocytes: Fine tuning between gap junctions and P2 nucleotide receptors in calcium wave propagation. *The Journal of Neuroscience*, *20*, 1435–1445. https://doi.org/10.1523/JNEUROSCI.20-04-01435.2000

Simon, A. M., & McWhorter, A. R. (2003). Decreased intercellular dye-transfer and downregulation of non-ablated connexins in aortic endothelium deficient in connexin37 or connexin40. *Journal of Cell Science*, *116*, 2223–2236. https://doi.org/10.1242/jcs.00429

Sims, C. E., & Allbritton, N. L. (1998). Metabolism of inositol 1,4,5-trisphosphate and inositol 1,3,4,5-tetrakisphosphate by the oocytes of Xenopus laevis. *The Journal of Biological Chemistry*, *273*, 4052–4058. https://doi.org/10.1074/jbc.273.7.4052

Smith, I. F., & Parker, I. (2009). Imaging the quantal substructure of single IP3R channel activity during Ca^{2+} puffs in intact mammalian cells. *Proceedings of the National Academy of Sciences*, *106*, 6404–6409. https://doi.org/10.1073/pnas.0810799106

Smith, I. F., Swaminathan, D., Dickinson, G. D., & Parker, I. (2014). Single-molecule tracking of inositol trisphosphate receptors reveals different motilities and distributions. *Biophysical Journal*, *107*, 834–845. https://doi.org/10.1016/j.bpj.2014.05.051

Smith, I. F., Wiltgen, S. M., Shuai, J., & Parker, I. (2009). Ca^{2+} puffs originate from pre-established stable clusters of inositol trisphosphate receptors. *Science Signaling*, *2*, ra77. https://doi.org/10.1126/scisignal.2000466

Sneyd, J., Charles, A. C., & Sanderson, M. J. (1994). A model for the propagation of intercellular calcium waves. *The American Journal of Physiology*, *266*, C293–C302. https://doi.org/10.1152/ajpcell.1994.266.1.C293

Suadicani, S. O., Brosnan, C. F., & Scemes, E. (2006). P2X7 receptors mediate ATP release and amplification of astrocytic intercellular Ca^{2+} signaling. *Journal of Neuroscience: The Official Journal of the Society for Neuroscience*, *26*, 1378–1385. https://doi.org/10.1523/JNEUROSCI.3902-05.2006

Tallini, Y. N., Brekke, J. F., Shui, B., Doran, R., Hwang, S., Nakai, J., Salama, G., Segal, S. S., & Kotlikoff, M. I. (2007). Propagated endothelial Ca^{2+} waves and arteriolar dilation in vivo. *Circulation Research*, *101*, 1300–1309. https://doi.org/10.1161/CIRCRESAHA.107.149484

Taylor, C. W., & Konieczny, V. (2016). IP3 receptors: Take four IP3 to open. *Science Signaling*, *9*, pe1. https://doi.org/10.1126/scisignal.aaf6029

Thillaiappan, N. B., Chakraborty, P., Hasan, G., & Taylor, C. W. (2019). IP3 receptors and Ca^{2+} entry. *Biochimica et Biophysica Acta BBA - Molecular Cell Research*, *1866*, 1092–1100. https://doi.org/10.1016/j.bbamcr.2018.11.007

Thomas, A. P., Bird, G. S., Hajnóczky, G., Robb-Gaspers, L. D., & Putney, J. W. (1996). Spatial and temporal aspects of cellular calcium signaling. *FASEB Journal: Official Publication of the Federation of American Societies for Experimental Biology*, *10*, 1505–1517.

Toma, I., Bansal, E., Meer, E. J., Kang, J. J., Vargas, S. L., & Peti-Peterdi, J. (2008). Connexin 40 and ATP-dependent intercellular calcium wave in renal glomerular endothelial cells. *American Journal of Physiology. Regulatory, Integrative and Comparative Physiology*, *294*, R1769–R1776. https://doi.org/10.1152/ajpregu.00489.2007

Uhrenholt, T. R., Domeier, T. L., & Segal, S. S. (2007). Propagation of calcium waves along endothelium of hamster feed arteries. *American Journal of Physiology. Heart and Circulatory Physiology*, *292*, H1634–H1640. https://doi.org/10.1152/ajpheart.00605.2006

Walker, J. W., Somlyo, A. V., Goldman, Y. E., Somlyo, A. P., & Trentham, D. R. (1987). Kinetics of smooth and skeletal muscle activation by laser pulse photolysis of caged inositol 1,4,5-trisphosphate. *Nature*, *327*, 249–252. https://doi.org/10.1038/327249a0

Wang, D., Wong, H.-K., Feng, Y.-B., & Zhang, Z.-J. (2014). 18beta-glycyrrhetinic acid induces apoptosis in pituitary adenoma cells via ROS/MAPKs-mediated pathway. *Journal of Neuro-Oncology*, *116*, 221–230. https://doi.org/10.1007/s11060-013-1292-2

Wang, S. S., Alousi, A. A., & Thompson, S. H. (1995). The lifetime of inositol 1,4,5-trisphosphate in single cells. *The Journal of General Physiology*, *105*, 149–171. https://doi.org/10.1085/jgp.105.1.149

Wilson, B. S., Pfeiffer, J. R., Smith, A. J., Oliver, J. M., Oberdorf, J. A., & Wojcikiewicz, R. J. H. (1998). Calcium-dependent clustering of inositol 1,4,5-trisphosphate receptors. *Molecular Biology of the Cell*, *9*, 1465–1478. https://doi.org/10.1091/mbc.9.6.1465

Wilson, C., Lee, M. D., & McCarron, J. G. (2016). Acetylcholine released by endothelial cells facilitates flow-mediated dilatation. *The Journal of Physiology*, *594*, 7267–7307. https://doi.org/10.1113/JP272927

Wilson, C., Saunter, C. D., Girkin, J. M., & McCarron, J. G. (2016a). Advancing age decreases pressure-sensitive modulation of calcium signaling in the endothelium of intact and pressurized arteries. *Journal of Vascular Research*, *53*, 358–369. https://doi.org/10.1159/000454811

Wilson, C., Saunter, C. D., Girkin, J. M., & McCarron, J. G. (2016b). Clusters of specialized detector cells provide sensitive and high fidelity receptor signaling in the intact endothelium. *FASEB Journal: Official Publication of the Federation of American Societies for Experimental Biology*, *30*, 2000–2013. https://doi.org/10.1096/fj.201500090

Wilson, C., Zhang, X., Lee, M. D., MacDonald, M., Heathcote, H. R., Alorfi, N. M. N., Buckley, C., Dolan, S., & McCarron, J. G. (2020). Disrupted endothelial cell heterogeneity and network organization impair vascular function in prediabetic obesity. *Metabolism*, *111*, 154340. https://doi.org/10.1016/j.metabol.2020.154340

Wölfle, S. E., Schmidt, V. J., Hoepfl, B., Gebert, A., Alcoléa, S., Gros, D., & de Wit, C. (2007). Connexin45 cannot replace the function of connexin40 in conducting endothelium-dependent dilations along arterioles. *Circulation Research*, *101*, 1292–1299. https://doi.org/10.1161/CIRCRESAHA.107.163279

Xu, A., Wang, Y., Xu, L. Y., & Gilmour, R. S. (2001). Protein kinase C alpha -mediated negative feedback regulation is responsible for the termination of insulin-like growth factor I-induced activation of nuclear phospholipase C beta1 in Swiss 3T3 cells. *The Journal of Biological Chemistry*, *276*, 14980–14986. https://doi.org/10.1074/jbc.M009144200

Zakrzewicz, A., Richter, K., Agné, A., Wilker, S., Siebers, K., Fink, B., Krasteva-Christ, G., Althaus, M., Padberg, W., Hone, A. J., McIntosh, J. M., & Grau, V. (2017). Canonical and novel non-canonical cholinergic agonists inhibit ATP-induced release of monocytic interleukin-1β via different combinations of nicotinic acetylcholine receptor subunits α7, α9 and α10. *Frontiers in Cellular Neuroscience*, *11*, 189. https://doi.org/10.3389/fncel.2017.00189

Zhang, X., Lee, M. D., Wilson, C., & McCarron, J. G. (2019). Hydrogen peroxide depolarizes mitochondria and inhibits IP3-evoked Ca^{2+} release in the endothelium of intact arteries. *Cell Calcium*, *84*, 102108. https://doi.org/10.1016/j.ceca.2019.102108

Zhu, D., Caveney, S., Kidder, G. M., & Naus, C. C. (1991). Transfection of C6 glioma cells with connexin 43 cDNA: Analysis of expression, intercellular coupling, and cell proliferation. *Proceedings of the National Academy of Sciences of the United States of America*, *88*, 1883–1887. https://doi.org/10.1073/pnas.88.5.1883

Zimmermann, B., & Walz, B. (1999). The mechanism mediating regenerative intercellular Ca^{2+} waves in the blowfly salivary gland. *The EMBO Journal*, *18*, 3222–3231. https://doi.org/10.1093/emboj/18.12.3222

SUPPORTING INFORMATION

Additional supporting information can be found online in the Supporting Information section at the end of this article.

How to cite this article: Buckley, C., Lee, M. D., Zhang, X., Wilson, C., & McCarron, J. G. (2024). Signalling switches maintain intercellular communication in the vascular endothelium. *British Journal of Pharmacology*, 1–23. https://doi.org/10.1111/bph.16366